Published online 25 September 2017 *Nucleic Acids Research, 2017, Vol. 45, No. 20* ***11989–12004***
doi: 10.1093/nar/gkx852

The basic tilted helix bundle domain of the prolyl isomerase FKBP25 is a novel double-stranded RNA binding module

David Dilworth[1,†], Santosh K. Upadhyay[2,3,4,†], Pierre Bonnafous[2,3], Amiirah Bibi Edoo[2,3], Sarah Bourbigot[2,3], Francy Pesek-Jardim[1], Geoff Gudavicius[1], Jason J. Serpa[1,5], Evgeniy V. Petrotchenko[1,5], Christoph H. Borchers[1,5], Christopher J. Nelson[1,*] and Cameron D. Mackereth[2,3,*]

[1]Dept. of Biochemistry and Microbiology, University of Victoria, Victoria, BC V8W 3P6, Canada, [2]Univ. Bordeaux, Institut Européen de Chimie et Biologie, 2 rue Robert Escarpit, F-33607 Pessac, France, [3]Inserm U1212, CNRS UMR 5320, ARNA Laboratory, Univ. Bordeaux, 146 rue Léo Saignat, F-33076 Bordeaux, France, [4]CSIR-Institute of Genomics and Integrative Biology, New Delhi 110020, India and [5]University of Victoria Genome BC Proteomics Centre, Vancouver Island Technology Park, Victoria, BC V8Z 7X8, Canada

Received May 02, 2017; Revised September 05, 2017; Editorial Decision September 12, 2017; Accepted September 13, 2017

ABSTRACT

Prolyl isomerases are defined by a catalytic domain that facilitates the *cis–trans* interconversion of proline residues. In most cases, additional domains in these enzymes add important biological function, including recruitment to a set of protein substrates. Here, we report that the N-terminal basic tilted helix bundle (BTHB) domain of the human prolyl isomerase FKBP25 confers specific binding to double-stranded RNA (dsRNA). This binding is selective over DNA as well as single-stranded oligonucleotides. We find that FKBP25 RNA-association is required for its nucleolar localization and for the vast majority of its protein interactions, including those with 60S preribosome and early ribosome biogenesis factors. An independent mobility of the BTHB and FKBP catalytic domains supports a model by which the N-terminus of FKBP25 is anchored to regions of dsRNA, whereas the FKBP domain is free to interact with neighboring proteins. Apart from the identification of the BTHB as a new dsRNA-binding module, this domain adds to the growing list of auxiliary functions used by prolyl isomerases to define their primary cellular targets.

INTRODUCTION

Proline is found in *cis* and *trans* peptide-bond conformations in proteins. These conformations differ by 180° in the Ω-angle of the peptide bond, and thus have a direct effect on the protein backbone structure. Because *cis* and *trans* conformers interconvert slowly on a second to minute timescale, prolyl-isomerization can limit the rate of protein folding (1). Three families of prolyl-isomerases catalyze the interconversion of prolyl conformers: FK506 binding proteins (FKBPs), cyclophilins and parvulins. These proteins serve either as *de novo* protein folding chaperones (2), or in a signalling context as regulators of folded proteins (3). Such targets of prolyl-isomerases are located throughout the cell: ion-channels (4,5); receptors (6); viral capsid proteins (7–9); signalling molecules (10); transcription factors such as p53 (11), Notch (12), and YY1 (13,14), RNA Polymerase II (reviewed in (15)), and histones (16–18) are each regulated by prolyl-isomerization. FKBP and cyclophilin family members are also the targets of the immunosuppressive drugs rapamycin and cyclosporine. While these molecules operate by forming FKBP–mTOR and Cyp–calcineurin drug-induced inhibitory complexes, respectively, their side effects may be mediated by interaction and inhibition of other prolyl isomerases. Knowledge of the proteins and processes regulated by each prolyl-isomerase is therefore critical in order to understand their native function, and to determine direct and off-target effects of therapeutic agents that target these proteins.

The prolyl-isomerase–substrate information is unfortunately lacking or incomplete for most family members, and the molecular basis for their target selectivity is unclear. It is assumed that protein-protein interactions, usually mediated by accessory domains, direct these enzymes to dis-

*To whom correspondence should be addressed. Tel: +33 540003432; Email: cameron.mackereth@inserm.fr
Correspondence may also be addressed to Christopher J. Nelson. Email: cjn@uvic.ca
†These authors contributed equally to this work as first authors.

crete subcellular locations and substrates (19). For example, while FKBP12 is a 12 kDa single domain cytosolic protein, the 25 kDa FKBP25 is predominantly found in the nucleus (20,21) where it interacts with nucleolin (20,21), MDM2 (22), HDAC1/HDAC2 (14), numerous ribosomal and ribosome biogenesis factors (21), and a subset of chromatin proteins (21). Recently, the N-terminal accessory domain of FKBP25 was found to adopt a novel basic tilted helix bundle (BTHB) domain fold (23) which mediates its interaction with YY1. A combined interface made by the BTHB and FKBP domains was also reported to bind to DNA, albeit with low affinity (24). Although the interaction with YY1, and possibly DNA, can explain some of the targets of FKBP25, what is missing is a defining property that accounts for the remaining putative substrates and most notably the proteins associated with the ribosome.

Here, we demonstrate that FKBP25 localization and protein interactions are each RNA-dependent and mediated by a direct and specific interaction between the BTHB domain and double-stranded RNA (dsRNA). We show that the dsRNA-binding domain functions independently of the catalytic FKBP domain, establishing a tether model in which the BTHB anchors FKBP25 to protein complexes containing dsRNA. In support of this model, we show that proteins near FKBP25 *in vivo* are enriched in RNA-binding proteins, ribosome subunits and maturation factors, as well other chromatin proteins. The direct association of the BTHB of FKBP25 with dsRNA thus brings this FKBP to a discrete substrate clientele of proteins in ribonucleoprotein complexes. The discovery of the BTHB domain as a new dsRNA-binding domain also adds a new member to the small number of domain folds known to recognize dsRNA.

MATERIALS AND METHODS

Plasmids

Expression vectors for stable integration, and tetracycline inducible expression, were generated by sub-cloning a synthesized FKBP25–3xFLAG-His_6 gene (GenScript) into a modified pcDNA5/FRT/TO vector (Thermo Fisher). FKBP25-FLAG-NLS vectors were constructed by PCR amplification of a FLAG-HA-NLS (FHN) tag from pcDNA4-FHN-4ICD (kindly provided by N. Yamaguchi, Chiba University) which was then subcloned into the pcDNA5 vector to replace the 3x-FLAG-6xHis tag (25). To create BirA fusion products, FKBP25 was cloned into pcDNA3.1 mycBioID (Addgene #35700) and pcDNA3.1 MCS-BirA(R118G)-HA (Addgene #36047) vectors.(26) Expression vectors for recombinant production of human FKBP25 in *Escherichia coli* were made by inserting constructs into NcoI/Acc65I sites in a modified pET-9d plasmid containing an N-terminal His_6 purification tag followed by a tobacco etch virus (TEV) protease cleavage site. Inserts include full-length FKBP25 (residues 1–224), as well as the isolated BTHB domain (1-74) and FKBP domain (108–224). The first two RRM domains from hamster nucleolin (residues 299–459) was expressed from a pET-15b plasmid (kindly provided by P. Bouvet, Ecole Normale Superieure de Lyon). Mutant proteins were created by using PCR amplification with a set of oligos overlapping the mutation site. All constructs were validated by sequencing.

Cell culture, plasmid transfection, and generation of stable cell lines

U2OS (ATCC HTB-96) and Flp-In T-Rex HEK293 (Thermo Fisher) cells were grown in a 5% CO_2 humidified incubator at 37°C in DMEM media supplemented with 10% (v/v) fetal bovine serum and antibiotics (10 μg/ml penicillin and 10 units/ml streptomycin). Transfection of DNA for both transient and stable expression was performed using Lipofectamine 3000 (Thermo Fisher) following the manufacturer's instructions. To generate stable cells expressing tagged FKBP25, Flp-In T-Rex HEK293 cells were transfected with a 9:1 ratio of pOG44 (Thermo Fisher) to pcDNA5 integration vector and allowed to recover for 24 h prior to selection with hygromycin (InvivoGen). Stable clones were pooled and tested for expression with the addition of 1 μg/ml tetracycline (Sigma) for 24 h. U2OS stable cell lines expressing BirA fusion proteins were created by transfection and clonal isolation following G418 selection (A.G. Scientific). Clones were screened by western blotting with streptavidin–horse radish peroxidase (Thermo Fisher).

Affinity capture of biotinylated proteins

Purification of biotyinatled proteins was performed as outlined by (26). U2OS cells stably expressing an FKBP25-BirA-HA fusion protein or Myc-tagged BirA control were incubated for 24 h in complete DMEM media supplemented with 50 μM biotin (Sigma) in 15 cm^2 dishes. Cells were then washed three times in PBS and lysed directly on the plate with 1 ml Lysis Buffer (50 mM Tris pH 7.4, 500 mM NaCl, 0.4% SDS, 5 mM EDTA, 1 mM DTT, and protease inhibitors consisting of 1 μg/ml leupeptin, 1 μg/ml aprotinin and 1 μg/ml pepstatin). Lysates were sonicated on high for cycles of 30 s with a 30 s rest, for a total time of 5 min on ice using a BioRupter (Diogenode). Triton X-100 was added to a final volume of 2% and the lysates were again sonicated as above. Lysates were then diluted in an equal volume of chilled 50 mM Tris pH 7.4 and subjected to a final round of sonication. Insoluble cellular debris was cleared by centrifugation at 16 000 x *g* for 10 min at 4°C. Cleared extracts were normalized by Bradford assay prior to loading on 125 μl slurry of washed Dynabeads MyOne Streptavidin C1 (Thermo Fisher) and incubated overnight at 4°C. The following morning, beads were washed two times with Wash Buffer 1 (2% SDS), once with Wash Buffer 2 (0.1% sodium deoxylcholate, 500 mM NaCl, 1 mM EDTA, 50 mM Hepes ph7.5, and 1% Triton X-100), once in Wash Buffer 3 (10 mM Tris pH 8.1, 250 mM LiCl, 0.5% NP-40, 0.5% sodium deoxycholate, and 1 mM EDTA), and finally two times with Wash Buffer 4 (50 mM Tris pH 7.4 and 50 mM NaCl), pelleting beads using a magnetic rack. For western blotting, beads were resuspended in Laemmli sample buffer supplemented with 50 μM biotin and boiled for 10 minutes before loading on an SDS-PAGE gel.

Immunoprecipitation

Expression of stably-integrated or transiently-transfected FKBP25 constructs was induced with 1 μg/ml tetracycline for 24 h prior to harvesting. For immunopreciptation experiments performed with nuclear extract, the extracts were prepared by resuspending cell pellets (~3×10^7 cells) in 1 ml buffer A (16.7 mM Tris pH 8, 50 mM NaCl, 1.67 mM $MgCl_2$, 0.1% Triton X-100 and protease inhibitors), vortexed for 10 s and incubated on ice for 5 min. Nuclei were centrifuged at 1000 x *g* for 5 min. Pellets were washed once more in buffer A as above. To extract the nuclear material, the pellet was sonicated using a BioRupter (Diagenode) on high power for cycles of 30 s with a 30 s rest, for a total time of 5 min on ice in 0.5 ml sonication buffer (25 mM Tris pH 8, 100 mM KCl, 2 mM EDTA, 1 mM DTT, 0.05% IGEPAL and protease inhibitors). Insoluble material was pelleted by centrifugation at 12 000 x *g* for 15 min. Extracts were normalized for total protein by Bradford assay. For immunopreciptations using whole cell extracts, cells were resuspended directly in immunoprecipitation wash buffer (50 mM Tris pH 8, 150 mM NaCl, 0.5% (w/v) NP-40, 0.5% (w/v) Triton X-100, 2 mM EDTA and protease inhibitors) and sonicated as above. Insoluble material was pelleted by centrifugation at 12 000 x *g* for 15 min and normalized by Bradford assay. For RNase A treatment, extracts (2–3 mg) were incubated with 100 μg RNase A (Qiagen) for 5 min at 37°C, followed by 1 h at 4°C. Nuclear and whole cell extracts were added to pre-washed EZ-view Red ANTIFLAG M2 Affinity gel beads (Sigma), and incubated at 4°C for 1.5–3 h with nutation. After binding, beads were washed three times in IP wash buffer. Bound FLAG-tagged FKBP25 and interacting proteins were eluted by competition with 3xFLAG peptide (Sigma), by nutating beads in 150 ng/μl peptide in 1× TBS for 20 min at 4°C. Eluted material was resolved by NuPAGE Novex 4–12% Bis–Tris gradient gels at 150 V for approximately 1.5 h and either silver stained, transferred to nitrocellulose membrane for western blotting, or further processed for mass spectrometry analysis.

Protein identification by mass spectrometry

BioID samples were processed for mass spectrometry as outlined by (27). Briefly, streptavidin beads were washed with 50 mM NH_4HCO_3 and resuspended in 50 mM NH_4HCO_3 containing 5 mM dithiothreitol and heated at 75°C for 10 min. Iodoacetamide was added to a final concentration of 10 mM to each sample followed by incubation in the dark at room temperature for 20 min. Afterward, 1 mM $CaCl_2$ and fresh 5 mM dithiothreitol were added and incubation continued overnight. The following morning, trifluoroacetic acid (TFA) was added to a final concentration of 0.5% (v/v). Beads were pelleted using a magnetic rack and the supernatant removed. A second elution of digested peptides with 0.5% TFA was performed and the supernatant pooled. To each sample, 1 μg of sequence-grade trypsin was added and incubated overnight at 37°C. For 3x-FLAG peptide eluted material, in-solution trypsin digests were performed by incubating samples with 1 μg of sequence-grade trypsin (Promega) at 37°C in 1× TBS followed by lyophilization until dry. Digested peptides were passed over ZipTips (Millipore) and eluted with 0.1% TFA/50% acetonitrile. Peptides were analyzed by an Orbitrap LTQ mass spectrometer (Thermo Scientific) with result searches performed using the program MASCOT (Matrix Science). To identify protein interactors, peptide counts for sample versus control were submitted to the Crapome web server (28). Proteins identified that had a fold change greater than two, and at least two peptides detected, were considered to be enriched.

Gene ontology & network analysis

For gene ontology analysis, lists of interacting proteins were submitted to the DAVID (Database for Annotation, Visualization and Integrated Discovery version 6.8) web server (29). Gene ontology terms with a P-value < 0.05 were then summarized using the REVIGO (reduce and visualize gene ontologies) (30) server using a similarity cutoff of 0.46. Network visualizations were generated using Cytoscape software with protein-interaction data from the APID (Agile Protein Interactomes DataServer) database (31,32).

Western blot

For western blotting, eluted proteins were resolved by SDS-PAGE and transferred to a nitrocellulose membrane with phosphate transfer buffer (50 mM sodium phosphate buffer pH 6.8, 15% EtOH). Membranes were blocked in 10% skim milk for 30 min and probed in primary antibody for either 1 h at room temperature or overnight at 4°C. Followed by three 10 min washes in TBS-T (1× TBS containing 0.1% Tween 20). For development of western blots, either a chemiluminescence or fluorescence based detection system was used. For chemiluminescence, horseradish peroxidase conjugated anti-mouse (GE) or anti-rabbit (GE) secondary antibody was used at 1:5000 in 1% milk/TBS-T, incubating blots for 1 h at room temperature, followed by washing in TBS-T. Proteins were detected using chemiluminescence HRP substrate (Millipore) and exposed to film. For fluorescence based detection, blots were incubated with either IRdye 800CW anti-mouse (Mendel Scientific) or IRdye 680RD anti-rabbit (Mendel Scientific) at 1:5000 for 1 h at room temperature in 1% milk TBS-T, followed by washing in TBS-T and imaging on an Odyssey Clx imaging system (Li-Cor).

Antibodies

The following antibodies were used in this study; FKBP25 (Genscript, epitope residues 201–224-IF 1:300, WB 1:2500), alpha-Tubulin (Rockland 600-401-880—WB 1:10000), Ku86 (Santa Cruz sc-9034—WB 1:5000), Ku70 (Millipore Q2187163—WB 1:2500), TopoI (AbCam ab109374—WB 1:10 000), Parp1 (Santa Cruz sc-8007—WB 1:5000), Nucleolin (AbCam ab22758—WB 1:5000), RPL3 (Santa Cruz sc-86828 - WB 1:500), RPS6 (Santa Cruz sc74459—WB 1:500), FLAG (Sigma F3165—WB 1:50000), RPL23a (Santa Cruz sc-135388—1:500) and UBF (Santa Cruz sc13125 X—IF 1:500).

Immunofluorescence

Cells were seeded on eight-well glass slides (Millipore) at least 24 h before fixation. For pre-extraction, cells were washed first with 1× PBS and then incubated twice for 3 min at room temperature with CSK+T (10 mM Pipes pH 7.0, 100 mM NaCl, 300 mM sucrose, 3 mM $MgCl_2$ and 0.5% Triton X-100) or CSK+T+R (CSK+T with 0.3 mg/ml RNase A) (33). CSK alone treated cells were washed with 1× PBS and CSK buffer without detergent or RNase A as above. To fix cells, they were first washed in 1× PBS and then incubated in a 3% paraformaldehyde solution in PBS, followed by three washes in 1× PBS. Before staining, cells were permeabilized for 10 min on ice using 0.5% Triton X-100 in 1× PBS and then blocked for 30 min in PBS-T (0.1% Tween 20 in PBS) containing 1% BSA at room temperature. Slides were then incubated with primary antibody diluted in PBS-T for 1 h at room temperature followed by three 5 min washes in PBS. After washing, the slides were then incubated with secondary antibodies, AlexaFluor 488 goat anti-mouse (Life Technologies) and goat anti-rabbit IgG-CFL 555 (Santa Cruz), in PBS-T for one hour and washed three times in 1× PBS. Coverslips were mounted using Fluoroshield with DAPI (Sigma) and sealed with clear nail polish. Slides were imaged on a SP8 confocal microscope (Leica) or BM IRE2 epifluorescence (Leica) and images processed using the Fiji distribution of ImageJ (34). Assays with actinomycin D included an incubation at 10 nM in DMSO for 4 h prior to pre-extraction with CSK+T. Incubation with DMSO was used as a control.

In vitro protein expression and purification

Full-length human FKBP25 (residues 1–224), along with truncation mutants corresponding to the isolated BTHB domain (1-74) or FKBP domain (108–224), were expressed in *Escherichia coli* BL21 *Lys Y* (New England Biolabs) using LB medium or M9 minimum medium supplemented with $^{15}NH_4Cl$ (1 g/l), and for ^{13}C-labelled protein supplemented also with ^{13}C-glucose (2 g/l). Protein expression was initiated at a OD (600 nm) of 0.6 with 0.5 mM IPTG (final concentration), and was followed by overnight incubation at 25°C. Bacteria were collected by centrifugation and resuspended in 20 ml per litre culture media with 50 mM Tris (pH 7.5), 500 mM NaCl, 5% (v/v) glycerol and 5 mM imidazole. Cell lysate preparation used a combination of lysozyme and sonication followed by centrifugation at 20 000 x *g* for 30 min. Protein purification from cell lysate was achieved by using Ni^{2+}-affinity chromatography with buffers composed of 50 mM Tris (pH 7.5), 500 mM NaCl, 5% (v/v) glycerol, and 5, 25 and 500 mM imidazole for the loading, wash and elution, respectively. Pooled fractions containing protein were exchanged to the low imidazole buffer by using a PD-10 column (GE Healthcare Life Sciences) and the His_6 tag was removed by addition of TEV protease and overnight incubation at 4°C. followed by a second Ni^{2+}-affinity chromatography step. The purified samples were concentrated by filter centrifugation, and the buffer exchanged by NAP-5 columns (GE Healthcare Life Sciences) into 20 mM sodium phosphate, pH 6.5 and 150 mM NaCl. Protein concentration was quantified by measuring the absorbance at 280 nm.

Oligonucleotide synthesis

The RNA was synthesized by using an Expedite 8909 (PerSeptive Biosystems). The DNA oligonucleotides were commercially produced (Eurogentec). Concentrations were determined by measuring absorbance at 260 nm with extinction coefficients from OligoAnalyzer 3.1 (eu.idtdna.com/calc/analyzer).

NMR spectroscopy and chemical shift assignment

NMR spectra were recorded at 298 K using a Bruker Avance III 700 MHz or 800 MHz spectrometers equipped with a triple resonance gradient standard probe or cryoprobe, respectively. Topspin versions 2.1, 3.2 and 3.5 (Bruker BioSpin) were used for data collection. Spectra processing used NMRPipe (35) followed by analysis with Sparky 3 (T.D. Goddard and D.G. Kneller, University of California) or NMRviewJ 8.0 (One Moon Scientific). Spectra for the assignment of backbone $^{1}H^{N}$, $^{1}H^{\alpha}$, $^{13}C'$, $^{13}C^{\alpha}$, $^{13}C^{\beta}$ and $^{15}N^{H}$ nuclei of full-length FKBP25 were collected on a 200 μM ^{13}C,^{15}N-labeled sample in 20 mM sodium phosphate (pH 6.5) with 150 mM NaCl, and 10% D_2O added for the lock. NMR spectra include 2D ^{15}N-HSQC, 3D HNCO, 3D HNCACO, 3D HNCA. 3D HNCOCA, 3D CBCACONH, and 3D HNCACB. $^{1}H^{N}$ and $^{15}N^{H}$ assignments for the full-length protein were used to assign ^{15}N-HSQC spectra recorded for isolated BTHB and FKBP domains in the same buffer (20 mM sodium phosphate, pH 6.5, with 150 mM NaCl). For the BTHB domain, the assignments were confirmed by measuring additional 3D HNCO and 3D HNCACB spectra on a 310 μM sample of ^{13}C,^{15}N-labeled protein. Assignments of asparagine and glutamine sidechain amides were confirmed by using a 3D ^{15}N-HSQC-NOESY spectrum (150 ms mixing time).

Titration experiments

Binding of FKBP25 constructs to oligonucleotide ligands was monitored by NMR spectroscopy on a Bruker Avance III 700 MHz spectrometer equipped with a triple resonance gradient standard probe at 298 K. The buffer was the same as for the chemical shift assignment experiments: 20 mM sodium phosphate (pH 6.5), with 150 mM NaCl, and 10% D_2O added for the lock. At the start of each titration the ^{15}N-labeled protein had a concentration of 100 μM in 20 mM sodium phosphate (pH 6.5), with 150 mM NaCl, and 10% D_2O added for the lock. Following reference 1D ^{1}H and 2D ^{15}N-HSQC spectra, the ligand was added from a concentrated stock to final concentrations of 25, 50, 75 and 100 μM, and at each point 1D ^{1}H and 2D ^{15}N-HSQC spectra were collected. The only exception was for the sample titrated with nucleolin-bound b2NRE stemloop. In this case a final titration point (100 μM ligand) was first assembled stepwise with confirmation of nucleolin binding to b2NRE stemloop by 1D ^{1}H NMR, prior to adding 100 μM final concentration of ^{15}N-labeled $FKBP25_{(1–74)}$. This sample was then serially diluted with free ^{15}N-$FKBP25_{(1–74)}$ (which was also used as the reference) in order to obtain all titration points.

Electrophoretic mobility shift assays

Observation of oligonucleotide binding to full-length FKBP25 and the K22M/K23M mutant used a Tris-glycine gel system (36). Samples were prepared in 20 mM Tris (pH 7.5), 150 mM potassium acetate, 1 mM EDTA and 10% glycerol, with bromophenol blue added to aid in gel loading. Cy3 labeling was incorporated into the forward strands of the 23 nt DNA and RNA during chemical synthesis. Double-stranded oligonucleotides were prepared with unlabelled reverse strands. For each assay, 100 nM of the Cy3-labelled single- or double-stranded oligonucleotide was used with increasing protein concentrations of 0.5, 1, 2, 5, 10, 20, 40, 60, 80, 100, 160, 300 and 500 μM. Protein was freshly prepared since extended storage or freezing results in undefined changes to protein fidelity. Polycrylamide gels were prepared with final concentrations of 10% acrylamide:bisacrylamide (37.5:1), 300 mM Tris–HCl (pH 8.8), 0.1% (w/v) ammonium persulfate and 0.1% (v/v) TEMED. After 10 min gel polymerization, the wells were cleaned and the gel pre-run at room temperature for 30 min at 100 V in running buffer containing 27 mM Tris, 192 mM glycine, 1 mM EDTA and pH 8.3. Following a second cleaning of the wells, 2 μl of each sample was loaded and the gel was run at 100 V for an additional 30 min at room temperature. Visualization of Cy3 fluorescence used a Typhoon Trio+ imager (GE Healthcare) with a 580 nm filter, 532 nm laser, normal sensitivity, photo multiplier tube setting of 500 V and 100 micron resolution. Preparation of images used ImageQuant TL v8.1.0.0 with default visualization parameters. Apparent K_D was obtained with the equation: $b + ((m - b)/(1 + (K_d/x)^n))$ in the program QtiPlot (Ion Vasilief), by fitting the curve of bound fractions determined by densitometric averages of three experiments to protein concentration (x), baseline value (b), maximum (m) and the Hill coefficient (n).

UV cross-linking and immunoprecipitation (CLIP)

FKBP25 RNA CLIP experiments were performed as described previously (37). Briefly, 80% confluent HEK293-TRex cells were transfected in six-well dishes and incubated overnight before being split to 10 cm^2 dishes. Cells were then induced with 0.1 μg/ml tetracycline and incubated for an additional 24 h to induce expression. Cells were washed once with 1× ice cold PBS and then irradiated with 150 mJ/cm^2 UV at 254 nm using a Stratalinker 2400 (StrataGene). Irradiated cells were then harvested by cell scraping, aliquoted into three equal volumes, and snap-frozen in liquid nitrogen and stored at -80°C until use. Thawed cell pellets were lysed in 1 ml lysis buffer (50 mM Tris–HCl pH 7.4, 100 mM NaCl, 1% NP-40, 0.1% SDS and protease inhibitors). To remove DNA, 2 μl of Turbo DNase (Ambion) was added to each sample. To digest unprotected RNA, either a high (1:500), medium (1:10 000) or low (1:50 000) concentration of 100 mg/mL RNaseA was added and samples were incubated for 3 min at 37°C followed by centrifugation at 22 000 × g for 20 min to pellet any insoluble material. Protein A/G agarose beads (Thermo Fisher) were prepared by washing three times in lysis buffer, followed by incubation for 1 h at 4°C with 5 μg mouse anti-FLAG antibody (Sigma). Unbound antibody was washed away with two additional washes in lysis buffer. Cleared nuclease treated cell lysates were added to prepared beads and rotated at 4°C for 2 h. Beads were then washed twice with high-salt buffer (50 mM Tris–HCl pH 7.4, 1 M NaCl, 1 mM EDTA, 1% NP-20, 0.1% SDS and 0.5% sodium deoxycholate) followed by two washes with wash buffer (20 mM Tris–HCl pH 7.4, 10 mM $MgCl_2$, and 0.2% Tween-20). The beads were then subjected to an additional three washes in high-salt wash buffer and three in wash buffer. The supernatant was removed and beads were then resuspended in 8 μl of 1× PNK buffer (70 mM Tris–HCl pH 7.6, 10 mM $MgCl_2$, 5 mM DTT) containing 0.4 μl PNK (NEB) and 0.8 μl of 5 mCi/ml ^{32}P-γ-ATP (Perkin Elmer). The reaction was incubated at 37°C for 5 min. The ^{32}P-labeled PNK mix was removed and beads were boiled in 1× Laemmli loading buffer and resolved on a 10% SDS-PAGE gel. Gels were dried and exposed to a Phosphorscreen (Molecular Dynamics) overnight and imaged with a Storm 820 scanner (Molecular Dynamics).

^{15}N relaxation

Amide ^{15}N T1 and T2 relaxation data were acquired at 700 MHz and 298 K by measuring a series of 2D ^{15}N-HSQC spectra on 300 μM full-length ^{15}N-FKBP25 with variable delays (38). The relaxation delays for T1 spectra were 10, 40, 80, 140,250, 400, 600, 800, 100, 1200 and 1500 ms, with repeat measurements at 10, 140, 250, 600 and 1000 ms for error estimation. Resulting delays for the T2 spectra were 12, 24, 36, 49, 61, 73, 85 and 97 ms, with repeat measurements at 12 and 73 ms for error estimation. T2 measurements were also performed on 100 μM ^{15}N-FKBP25 bound to 100 μM dsRNA-23bp using the same parameters. Steady-state heteronuclear $\{^1H\}^{15}N$-NOE spectra were recorded with and without 3 s of ^{1}H saturation and represents an average of two separate samples. Relaxation rates and error calculations were determined using NMRViewJ (39).

Paramagnetic relaxation enhancement

In order to attach the paramagnetic compound, three mutants of FKBP25 were generated to introduce surface accessible cysteine residues (Q14C, T69C and T151C). The location of the introduced cysteines were also based on analysis of a previous structure of full-length FKBP25 (24). To prepare the samples, protein expression and purification was as described above, followed by 16 h incubation of the mutant proteins in 2 mM dithiothrietol. The buffer was then changed to 50 mM Tris (pH 8.0) with 150 mM NaCl by using a PD10 column (GE Healthcare Life Sciences). Five molar equivalents of 4-(2-iodoacetamido)-2,2,6,6,tetramethyl-1-piperidinyloxy (TEMPO) free radical dissolved in methanol was then added. After incubation in the dark for two hours, the samples were dialyzed for 16 h into 20 mM sodium phosphate (pH 6.5) with 150 mM NaCl by using 3.5 kDa MWCO dialysis tubing. After acquiring a reference ^{15}N-HSQC spectrum for each sample in the paramagnetic state, five molar equivalents of pH 6.5 ascorbic acid was added and left for 2 h, after which a second diamagnetic state ^{15}N-HSQC was collected. The paramagnetic relaxation enhancement (PRE) was calculated as the ratio of the backbone amide data heights for the paramagnetic over diamagnetic spectra.

RESULTS

RNA mediates the majority of FKBP25 protein–protein interactions

In order to better understand the function of FKBP25, we decided to first obtain information on proteins that come into close physical contact to FKBP25 in the cell. To this end, we used a proximity-dependent biotin identification (BioID) strategy to provide an historical snapshot of neighboring proteins. BioID utilizes a protein fusion to the promiscuous biotin ligase BirA to enable biotinylation of exposed primary amines, predominately lysines, on closely associated proteins in the presence of exogenous biotin (Figure 1A) (26). The biotin-tagged protein neighbors are then selectively purified via streptavidin capture and the digested peptides subsequently identified by mass spectrometry. We generated U2OS cell lines stably expressing either a FKBP25-BirA fusion protein or BirA alone. Cells were incubated for 24 h with biotin to allow labelling of proximal interactors and biotinylated proteins were purified by streptavidin capture under denaturing conditions (Figure 1B). Unbiased mass spectrometry protein identification revealed 73 proteins enriched in the FKBP25-BirA sample relative to the BirA control (Figure 1C). Gene ontology (GO) analysis of proximal interactors with the DAVID webserver (30) showed a strong enrichment for RNA binding and ribosome biogenesis factors, including 22 ribosomal proteins and several proteins involved in the early maturation events of ribosome production (Supplementary Table S1). We had previously identified a similar enrichment of ribosome biogenesis factors in an orthoganol proteomic screen based on immunoprecipitation of flag-tagged FKBP25 from HEK293 cells (21). We now show that many of these proteins are not merely found in large multiprotein complexes that contain FKBP25; rather, their biotinylation shows that they must be in close proximity to FKBP25 *in vivo*. Apart from proteins related to the ribosome, there is additional enrichment of other RNA-binding functions including proteins implicated in binding to polyA RNA, double-stranded RNA and mRNA 5′ UTRs (Figure 1D). The common aspect of RNA-binding behavior to most of the identified FKBP25 interactors suggests that RNA molecules may be a key mediator of these FKBP25 protein associations.

To test this hypothesis, we performed co-immunoprecipitation of FLAG-tagged FKBP25 from HEK293 nuclear extract without and with pre-treatment with RNase A. Silver staining of the immunoprecipitated material showed a clear reduction in co-purifying proteins to near background levels with RNase A pre-treatment (Figure 1E). These samples were then analyzed by mass spectrometry to precisely identify the RNA-dependent interactome of FKBP25 (Figure 1F and Supplementary Table S2). We found that RNaseA treatment disrupted the majority of protein interactions detected in our previous mass spectrometry screen (21), including those associated with early rRNA biogenesis and RNA metabolism (Figure 1G).

The overlap of proteins identified by the BioID and RNA-dependent Co-IP reveals a list of 12 common targets (Figure 1G and Supplementary Table S3) with a noticeable cluster of nine subunits of the 60S ribosome (RPL13, RPL15, RPL24, RPL27, RPL27A, RPL28, RPL3, RPL36, RPL8) and two subunits of the 40S ribosome (RPS23, RPS3A). An analysis of the complete FKBP25 interactome utilizing protein–protein interaction data from the Agile Protein Interactomes Dataserver (APID) (32) highlights the biological process clusters related to ribosome biogenesis and RNA metabolism (Supplementary Figure S1). We independently validated several of these interactions by western blot (Supplementary Figure S2), confirming that all interactions tested require intact RNA. A second observation from these studies is that inclusion of a canonical nuclear localization signal improves the capture of proteins from the BioID and proteomic screens. In keeping with previous results (21), this finding shows that the majority of FKBP25 protein-protein interactions occur within the nucleus, and that RNA-dependent interactions mainly derive from this nuclear pool of FKBP25.

Nucleolar localization requires RNA

To investigate a cellular link between RNA and nuclear FKBP25, we first performed *in situ* subcellular fractionations by treating cells with a mixture of detergent and buffered sucrose known as cytoskeleton buffer (Figure 2A; CSK); a technique commonly used to release soluble proteins prior to immunofluorescence to facilitate the visualization of proteins associated with large macromolecular complexes in the nucleus (26,40,41). A subset of FKBP25 from the CSK treatment is also found in this Triton-treated fraction (Figure 2A; CSK+T) which retains pre-ribosomes and chromatin-associated factors. Additional treatment with RNase A eliminates all remaining FKBP25 (Figure 2A; CSK+T/R), whereas proteins such as the core histones are retained. The inclusion of FKBP25 in the Triton-treated fraction is therefore dependent on RNA.

We then visualized the same treatments by confocal immunofluorescence microscopy in U2OS cells. CSK treatment alone, leaving cellular membranes intact, shows that FKBP25 is distributed throughout the cell (Figure 2B) in keeping with previous reports of FKBP25 shuttling between the nucleus and cytoplasm (22). In contrast, the addition of Triton, which permeabilizes cell membranes, eliminates soluble cytoplasmic and nuclear FKBP25 signal, leaving only the chromatin-associated fraction. We observe a distinctive pattern of FKBP25 clusters within the nucleus that are reminiscent of nucleoli, the nuclear substructures where early events in ribosome production take place (42,43). Indeed, co-localization with the rRNA transcription factor UBF confirms a nucleolar enrichment of FKBP25 (Figure 2B). This localization is efficiently disrupted with treatment by RNase A, whereas UBF, which is incorporated into nucleolar chromatin, remains intact. Furthermore, treatment of cells with actinomycin D, which blocks RNA polymerase I transcription of rRNA, reduces FKBP25 retention in the nucleolus (Figure 2C). Together, these results strongly indicate that FKBP25 is recruited to sites of nascent rRNA transcription through direct interaction with RNA. Given the importance of RNA in mediating protein-protein interactions and the dependence of RNA in nucleolar localiza-

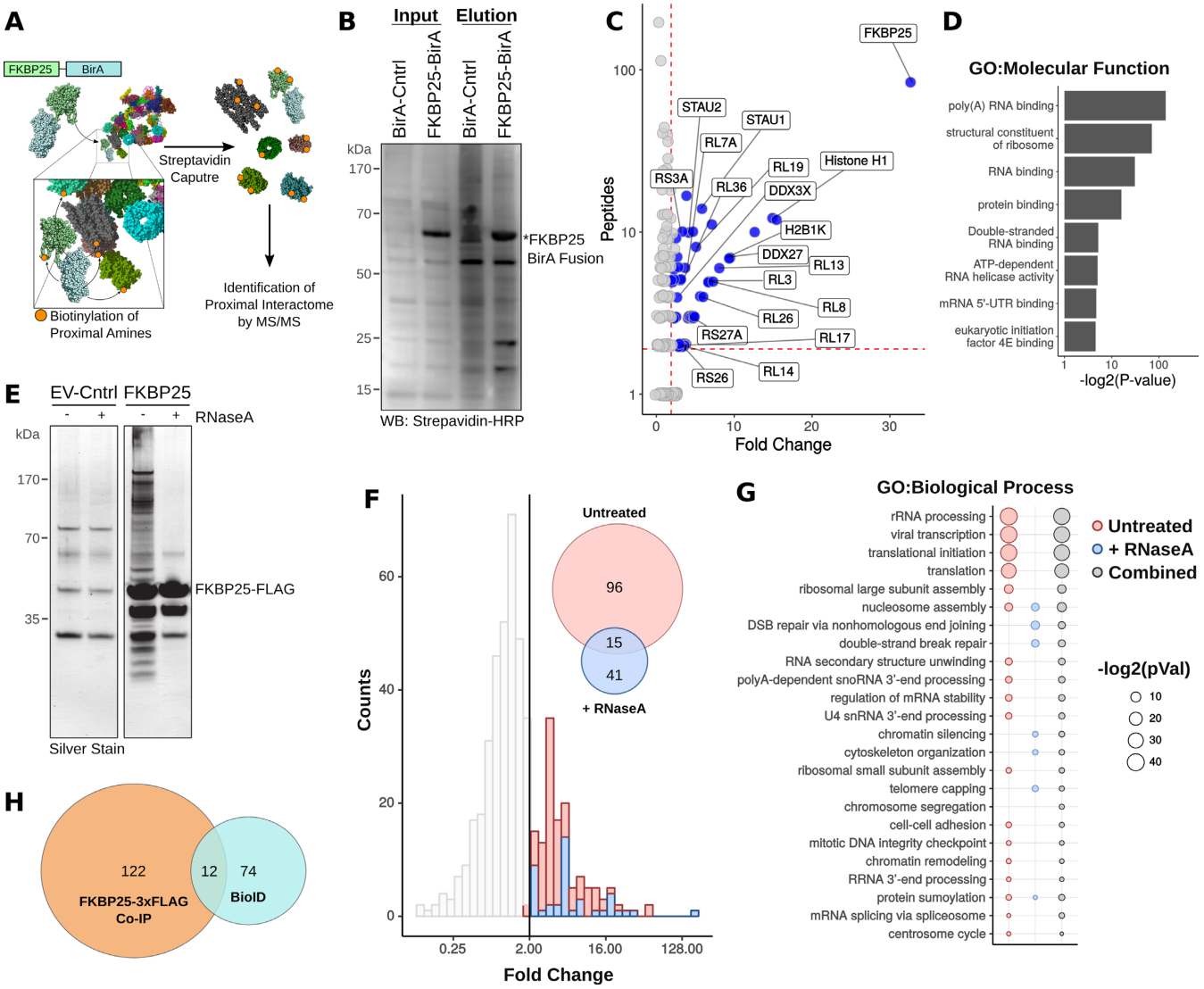

Figure 1. FKBP25 associates with ribosome biogenesis factors and other proteins in an RNA-dependent manner. (**A**) Schematic of BioID-based identification of cellular proteins proximal to FKBP25. (**B**) Streptavidin-HRP western blot of whole cell extracts and streptavidin capture from U2OS cells stably expressing an FKBP25 biotin ligase fusion or biotin ligase control, incubated for 24 hours in media containing 50 μM biotin. (**C**) Mass spectrometry identification of biotinylated proteins enriched in FKBP25-BirA streptavidin purifications relative to BirA control. The number of significant peptides identified relative to fold change is shown. (**D**) Enriched gene ontologies by molecular function. (**E**) FKBP25 3xFLAG-tagged co-immunoprecipitated material with and without pre-treatment with RNaseA analyzed by SDS-PAGE and visualized by silver stain. Empty vector cell lines are shown as a control. (**F**) Mass spectrometry analysis of proteins enriched in the FKBP25-FLAG sample relative to control, for samples either untreated or pre-treated with RNaseA. (**G**) Summarized gene ontology analysis by biological process. (**H**) Overlap in identified proteins between the BioID and FLAG co-immunoprecipitation experiments.

tion, we wondered if FKBP25 could in fact directly associate with RNA.

FKBP25 directly binds to RNA

Past studies have described direct binding of FKBP25 to DNA using a variety of techniques (13,24,44,45), and we first decided to replicate these findings by NMR spectroscopy. Using the 23 bp double-stranded DNA (dsDNA) ligand based on the transcription factor YY1 binding site (24), we observed movement of several amide crosspeaks in a series of 2D ^{15}N-HSQC spectra collected with increasing amounts of DNA (Figure 3A and Supplementary Figure S3) indicating residue-specific proximity to the ligand. This is in agreement with the recent report on DNA binding by FKBP25 (24). The modest shift for a subset of amide crosspeaks demonstrated weak but specific binding to residues in both the N-terminal (e.g. K22, K23, K48) and C-terminal (e.g. K154) domains. Given the importance of RNA in the function of FKBP25, we decided to repeat this experiment but with a double-stranded RNA (dsRNA) version of the 23 bp ligand (Figure 3A and Supplementary Figure S3). Strikingly, we saw a strong and specific association of the N-terminal region of FKBP25 to this ligand. Amide crosspeaks corresponding to the N-terminal domain of FKBP25 are broadened and undetected upon binding to the large

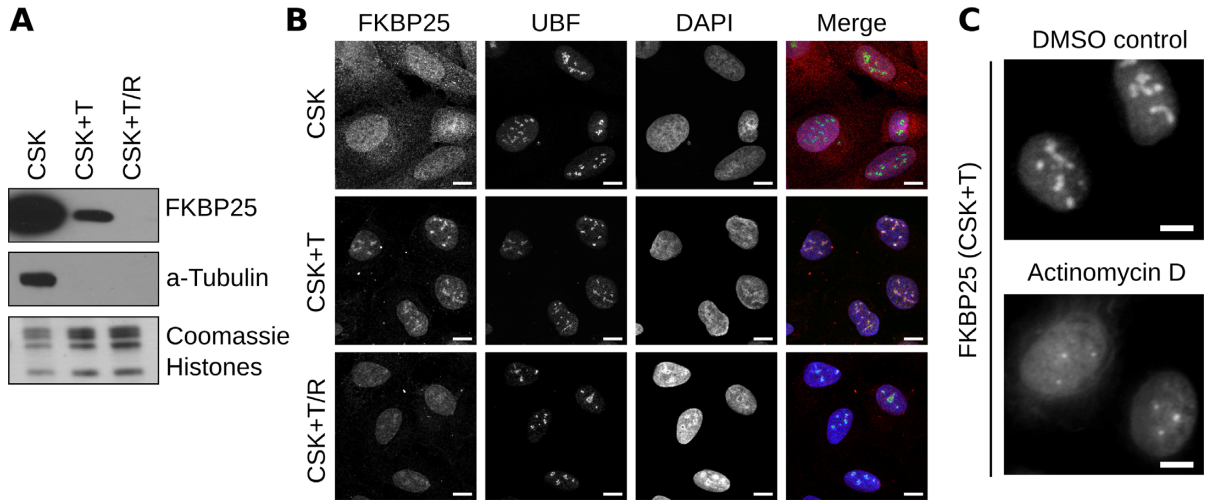

Figure 2. FKBP25 requires RNA for nucleolar localization. (**A**) Western blot analysis of U2OS cells following CSK treatment, with an additional Triton wash or a combination of Triton and RNaseA treatment. (**B**) Confocal microscopy of FKBP25 and the nucleolar-specific upstream binding factor (UBF). Cells were either untreated (CSK), pre-extracted with Triton (CSK + T), or pre-extracted with Triton and treated with RNaseA (CSK + T + R) prior to fixation. Scale bar is 10 μm. (**C**) Epi-fluorescence microscopy of FKBP25 in cells treated with DMSO or the RNA polymerase I inhibitor actinomycin D (10 nM for 4 h) and pre-extracted with CSK-T. Scale bar is 5 μm.

dsRNA ligand, whereas the linker and C-terminal domain remain visible with the same weak interaction to dsRNA as with dsDNA.

Using a complementary approach, we performed an electrophorectic gel mobility shift assay with the full-length FKBP25 and again find that a defined complex is made between FKBP25 and dsRNA-23bp (Figure 4A), with an apparent K_D of 122±8 μM. In agreement with the NMR data, the interaction with dsDNA is significantly weaker (Figure 4B). Further assays to define ligand preferences show no detectable binding to single-stranded RNA or DNA (Figure 4C and D), whereas FKBP25 is able to bind to an RNA/DNA duplex (Figure 4E).

In the NMR experiments, there is also an indication that the recognition of dsRNA may be limited to a specific region of FKBP25. To confirm a domain-specific interaction with dsRNA, we repeated the titrations with the isolated N-terminal basic tilted helix bundle (BTHB) domain from FKBP25 (residues 1–74). A strong chemical shift perturbation with dsRNA is maintained for the isolated BTHB domain (Figure 3B). Due to the smaller size of the isolated domain, more peaks are visible during the titration. Nevertheless, the same residues display ligand-specific chemical shift perturbation with magnitudes comparable to the full-length protein (Figure 3D). The isolated BTHB domain also maintains a weak interaction to dsDNA (Figure 3B) similar in magnitude and clustered to the same residues as for the full-length protein (Figure 3E). Titrations with the isolated C-terminal FKBP peptidyl prolyl isomerase domain from FKBP25 (residues 108–224) also recapitulated the findings from the full-length protein with weak interaction with both dsDNA and dsRNA (Figure 3C–E). Finally, co-immunoprecipitation experiments with separated N- and C-terminal regions of FKBP25 show that only the BTHB-containing construct retains association with the FKBP25 interaction partners nucleolin and RPL3 (Supplementary Figure S4). Together, these results point to a selective recognition of dsRNA by the BTHB domain of FKBP25. This specific binding is in contrast to the modest interaction to dsDNA by both domains. Also evident is a clear independence of the two domains with respect to nucleic acid binding, with similar binding behaviour displayed by the isolated domains and the full-length protein.

The BTHB domain is selective for dsRNA

The apparent selectivity of the BTHB for dsRNA over dsDNA prompted us to further probe the binding preferences of this domain with a variety of RNA and DNA oligonucleotides. Using the same approach as in Figure 3B we added increasing amounts of oligonucleotide to ^{15}N-labelled FKBP25$_{(1–74)}$ and monitored binding-induced changes in residue-specific NMR crosspeak positions or signal disappearance due to broadening (ligand sequences and selected spectra regions shown in Figure 5; full spectra in Supplementary Figure S5).

Given our previous data on FKBP25 interactions (21), as well as the results presented in Figures 1 and 2, we speculated that regions of double-stranded ribosomal RNA (rRNA) represent likely physiological ligands for the BTHB. In particular, we noted the previous link of FKBP25 to binding of the 28S rRNA in the pre-60S ribosomes (21). The 28S rRNA has numerous dsRNA segments within stemloop structures, and we selected two examples for which NMR spectroscopy data are already available (46). Titration of the BTHB domain with the b1 nucleolin recognition element (b1NRE) stemloop indeed resulted in chemical shift perturbation for similar residues as for the dsRNA-23bp ligand, and a comparable interaction was also observed with the b2NRE stemloop (Figure 5 and Supplementary Figure S5). Both stemloops were originally studied due to their interaction with nucleolin, and nucleolin was previously found in FKBP25-containing complexes (20,21). We therefore prepared a second b2NRE ligand pre-bound

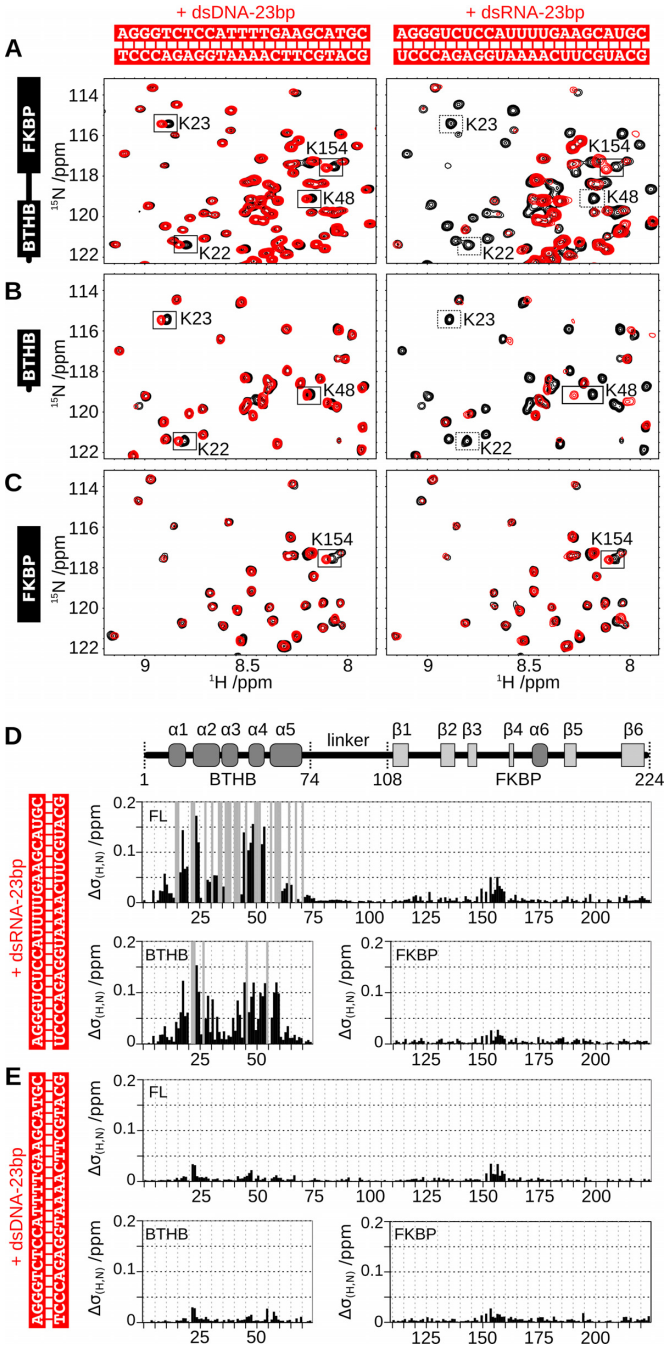

Figure 3. The BTHB domain displays binding preference for dsRNA over dsDNA. (**A**) ^{15}N-HSQC spectra regions corresponding to 100 μM ^{15}N-labeled full-length FKBP25 (in black) superimposed by the spectra with 100 μM added 23-bp dsDNA (left, in red) or 100 μM added 23-bp dsRNA (right, in red). Crosspeaks corresponding to three lysine residues from the BTHB domain (K22, K23, K48) and one from the FKBP domain (K154) have been annotated. Most crosspeaks corresponding to the BTHB domain broaden below detection upon addition of dsRNA-23bp. Full spectra in Supplementary Figure S3. (**B** and **C**) Similar analysis with the isolated BTHB domain (residues 1–74) and the isolated FKBP domain (residues 108–224). Full spectra in Supplementary Figure S3. (**D** and **E**) Combined $^{1}H^{N}$ and ^{15}N chemical shift perturbation for backbone amides in 100 μM samples of full-length FKBP25, BTHB domain or FKBP domain constructs upon addition of (D) 100 μM dsRNA-23bp or (E) dsDNA-23bp. Residue crosspeaks that are not observed in the ligand-bound complexes due to line-broadening are indicated with a grey bar. The secondary structure of FKBP25 is illustrated at the top.

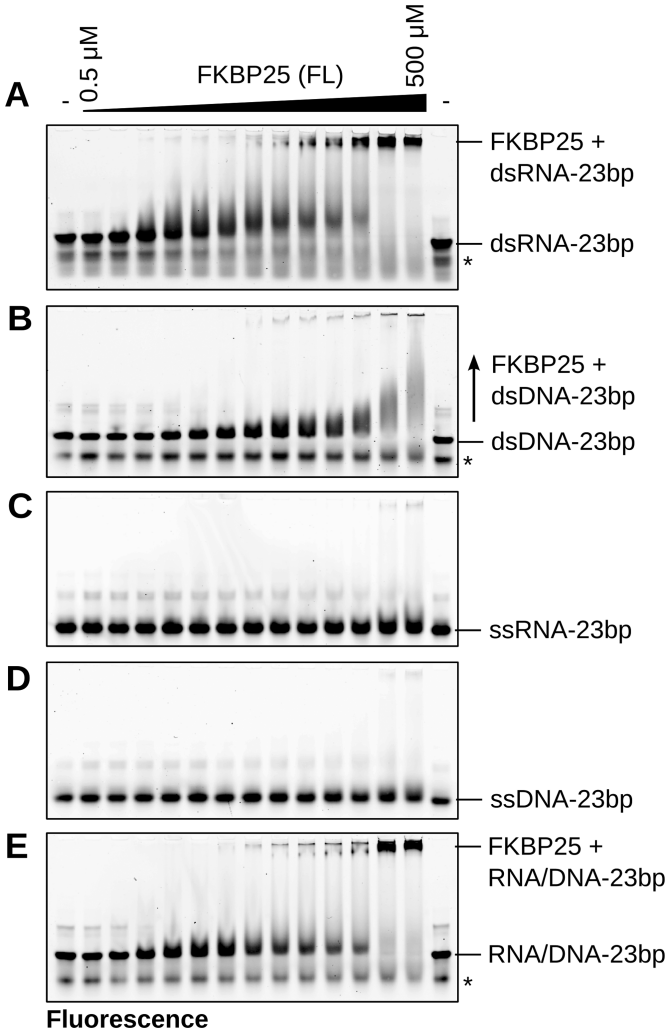

Figure 4. Binding preference for full-length FKBP25. (**A**–**E**) Electrophoretic mobility shift assays with 100 nM Cy3-labelled oligonucleotides and varying concentrations of FKBP25 from 0.5 to 500 μM. The first and last lanes of each gel do not contain protein. The migration of the free oligonucleotides as well as defined complexes are indicated. The asterisk denotes a minor contaminating species from the oligonucleotide synthesis.

to the first and second RNA recognition motif (RRM) domains of hamster nucleolin (residues 299–459). The presence of nucleolin on the b2NRE stemloop did not appear to affect the ability to bind to FKBP25. Detailed study of the stepwise assembly of the BTHB:b2NRE:nucleolin ternary complex reveals that there is little change in the NMR spectra of the RNA-bound BTHB without or with the addition of nucleolin, and likewise no significant perturbation of the RNA-bound nucleolin spectra following BTHB addition (Supplementary Figure S6). The BTHB domain thus appears to bind the dsRNA region of the b2NRE independent of nucleolin RRM1-RRM2 domains bound to the loop region. We conclude that dsRNA within the context of nucleolin-related stemloops provides one possible cellular target of the FKBP25 BTHB domain.

We next designed a short 8 bp oligonucleitde sequence to further characterize the binding specificity of the BTHB

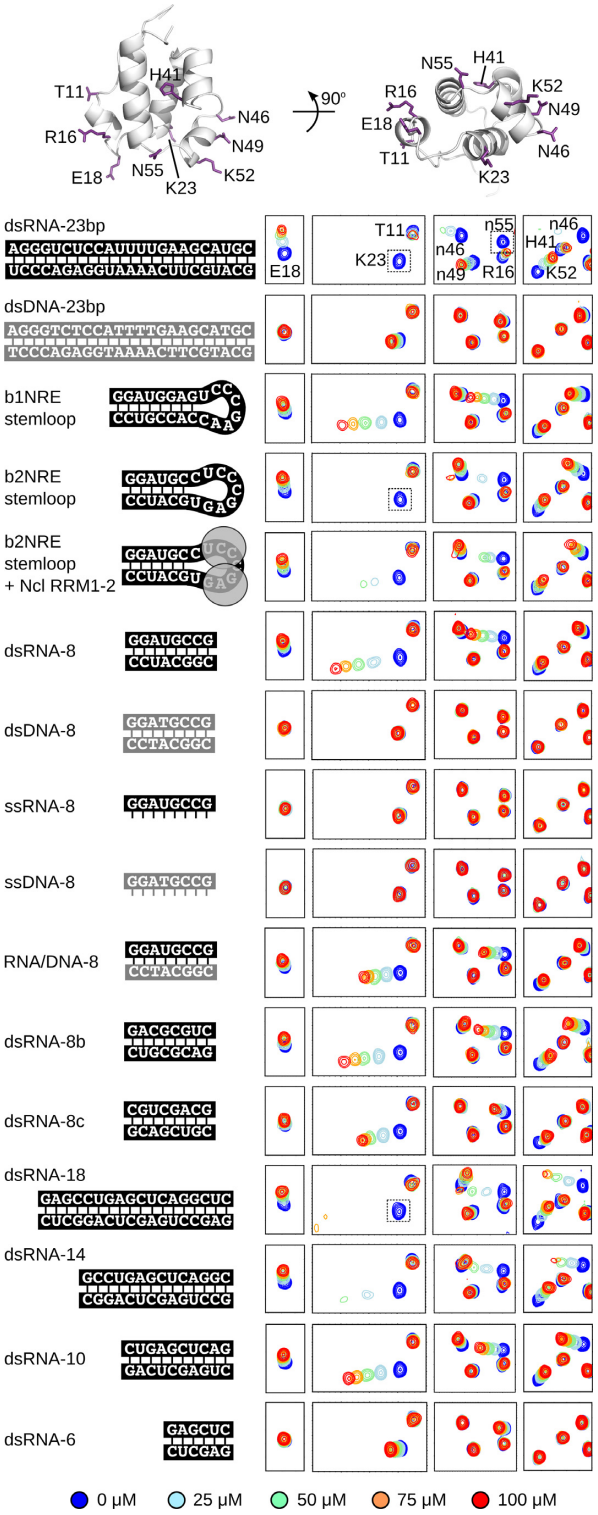

Figure 5. Binding preference for the isolated BTHB domain. Regions of NMR spectra following titration of various ligands into 100 μM ^{15}N-labelled FKBP25$_{(1–74)}$. The unbound spectrum is shown in blue, and the spectra following addition of 25, 50, 75 and 100 μM ligand are coloured light blue, light green, orange and red, respectively. The location of residues from the BTHB with annotated crosspeaks are indicated (top panel; atomic coordinates from PDB ID 2KFV) (23). Annotations with a small letter *n* correspond to the asparagine sidechain amide crosspeaks. Dotted boxes indicate peaks that broaden below detection upon addition of ligand. Full spectra are in Supplementary Figure S4.

domain. We based this ligand on the stem portion of the b2NRE ligand, and replaced the loop with two G–C basepairs. This ligand (dsRNA-8) was bound by the same residues sensitive to addition of the parent b2NRE stem-loop, as well as the longer dsRNA-23 bp (Figure 5 and Supplementary Figure S5). Specificity is also retained in the 8 bp ligand since the DNA version, dsDNA-8, did not result in any noticeable interaction. We then tested BTHB binding with the single-stranded oligonucleotides ssRNA-8 and ssDNA-8, neither of which showed signs of interaction. Finally, we found that an RNA–DNA duplex, RNA/DNA-8, was recognized by FKBP25 with similar but reduced changes in the NMR spectra as for dsRNA-8 (Supplementary Figure S7A). Collectively, these results show that the isolated BTHB domain recapitulates the binding preference of full-length FKBP25 to dsRNA and to an RNA–DNA duplex. The isolated BTHB domain does not bind ssRNA, ssDNA or dsDNA.

The ability of FKBP25 to interact with dsRNA-23bp, b1RNE, b2NRE and dsRNA-8 already suggests that the BTHB domain lacks sequence specificity for dsRNA binding. To further address this aspect, we designed two new 8 bp ligands with varying palindromic sequences. Both dsRNA-8b and dsRNA-8c were bound by the BTHB, with dsRNA-8b resulting in chemical shift perturbation of a similar magnitude to dsRNA-8 whereas dsRNA-8c results in reduced spectral changes (Figure 5 and Supplementary Figure S7A). There is also indication of some ligand- and residue-specific effects (Supplementary Figure S7B), such as the large perturbation of the Asn46 side chain amide only for dsRNA-8b. Therefore, although there is a general lack of sequence specificity, the BTHB may still possess a degree of uncharacterized sequence or shape preference that could target a distinct set of RNA targets.

Finally, we asked if BTHB-dsRNA affinity is influenced primarily by the length of the dsRNA. From the NMR spectroscopy titrations, it was already shown that the 8 bp dsRNA ligand results in less perturbation as compared to the original dsRNA-23 bp. We therefore tested an additional series of four palindromic ligands from 6 bp to 18 bp (Figure 5 and Supplementary Figure S5). A comparison of amide crosspeak positions reveal highest changes for dsRNA-18 and dsRNA-14, with reduced changes for dsRNA-10 and only minimal perturbation by dsRNA-6 (Supplementary Figure S7C). Competition mobility shift assays confirm a diminishing affinity with decreasing ligand size (Supplementary Figure S7D). It therefore appears that binding affinity is sensitive to the length of the dsRNA, which is consistent with an affinity driven by multivalent and non-specific interactions (47,48) that increase with the length of dsRNA. The results also demonstrate that association with FKBP25 requires a dsRNA ligand longer than 6 bp.

RNA-binding ability is required for *in vivo* interactions of FKBP25

Our NMR studies provide information of the surface residues on the BTHB domain that are in close proximity to the dsRNA (Figure 6A and Supplementary Figure S8A). These include two pairs of lysine residues: K22/K23

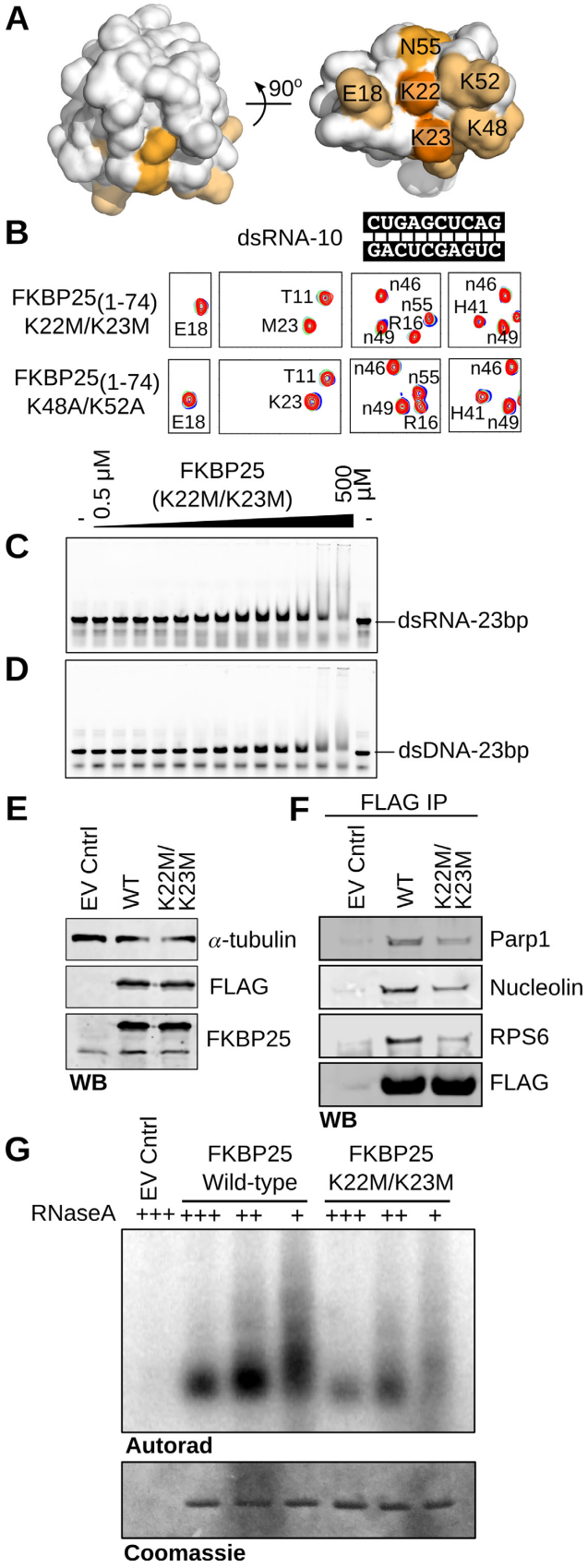

Figure 6. Mutation of key lysine residues reduces *in vitro* and cellular RNA-binding. (**A**) Residue amides in FKBP25$_{(1–74)}$ that are strongly and moderately affected by titration with dsRNA-10 are coloured in orange and light orange, respectively. Orientations of the domain in the image are the same as in Figure 5. Chemical shift perturbation details are in Supplementary Figure S8A. (**B**) NMR spectra following titration of dsRNA-10 into 100 μM ^{15}N-labeled FKBP25$_{(1–74)}$ with the K22M/K23M or K48/K52A mutations. Colours as in Figure 5. (**C** and **D**) Electrophoretic mobility shift assays with varying concentrations of full-length FKBP25 (K22M/K23M) as in Figure 4A and B. (**E**) Western blot analysis of FLAG-tagged FKBP25 constructs (wild-type and the K22M/K23M mutant) relative to endogenous FKBP25 (empty vector control) in HEK 293 cells. Antibodies against α-tubulin, FLAG-tag and FKBP25 correspond to the loading control, detection of FKBP25 constructs, and detection of both endogenous and FKBP25 constructs, respectively. (**F**) FLAG-affinity capture of cells expressing an empty vector control, wild-type FKBP25, or the K22M/K23M mutant with analysis by western blot using antibodies against the FKBP25-interacting proteins Parp1, nucleolin and RPS6. FKBP25 construct expression verified by antibodies against the FLAG tag. (**G**) RNA cross-linking IP (CLIP) experiment with wild-type FKBP25 or the K22M/K23M mutant in HEK293 cells, with DNAse pre-treatment coupled with variable amounts of RNase A.

and K48/K52. With an aim to design mutants for *in vivo* studies, we constructed two variants of FKBP25 targeting these lysine residues implicated in RNA binding. The double mutations K22M/K23M or K48A/K52A do not affect the folding of the BTHB domain as evident by their NMR spectra (Supplementary Figure S8B). Using the dsRNA-10 ligand we titrated each of the mutants and followed the binding using NMR spectroscopy. Both the K22M/K23M and K48A/K52A mutations greatly inhibited association with dsRNA (Figure 6B and Supplementary Figure S8C). We further tested the K22M/K23M mutant within the context of full-length FKBP25 and find that this mutation effectively eliminates the specificity for dsRNA (Figure 6C). The affinity to dsRNA is greatly reduced from the wildtype (Figure 4A) and is now similar in magnitude to a weak interaction with dsDNA (Figure 6D). The residual affinity to dsRNA and dsDNA is likely due to non-selective binding by the FKBP domain, as observed in the NMR titrations (Figure 3).

To confirm that FKBP25 does indeed interact directly with RNA in cells, we performed UV cross-linking immunoprecipitation (CLIP) experiments using both wild-type FKBP25 and the K22M/K23M mutant. UV cross-linking of cells results in irreversible covalent bonds between RNA binding proteins and their bound RNA, allowing stringent purification (49,50). We utilized FLAG-tagged Tet-inducible constructs to temper over-expression of the FKBP25 transgenes in order to limit the potential of a false positive interaction with RNA (Figure 6E). By treating extracts with either RNase or DNase, and radiolablelling any residual nucleic acids present in FKBP25 immunoprecipitates, we confirm that FKBP25 associates with RNA *in vivo* (Figure 6G). Further, the K22M/K23M mutant shows a significant reduction in the amount of directly bound RNA, highlighting the importance of these residues in mediating dsRNA-binding activity. Finally, we utilized this construct in Co-IP experiments and show a reduction in several FKBP25 binding partners relative to the wild-type sequence (Figure 6F). We therefore demonstrate that the mutation of two key lysine residues in the BTHB reduces

RNA binding *in vitro* and in cells, with a confirmed reduction in RNA-dependent protein interactions.

The BTHB and FKBP domains are structurally independent

The various *in vitro* and cellular experiments illustrate an independent behaviour of the two folded domains regarding nucleic-acid binding. However, this independence is inconsistent with a previous NMR spectroscopy study of FKBP25 in which intermolecular contacts bind these domains into a single structural unit (24). We have used NMR spectroscopy to study the nature of FKBP25, starting with the use of ^{15}N relaxation to identify regions of conformational disorder in the protein backbone. In the measurement of heteronuclear $\{^1H\}^{15}N$ relaxation, residues with a value greater or less than 0.5 correspond to rigid or flexible regions of the protein, respectively (Figure 7A). The data confirm the rigid nature of the two domains, with flexible regions limited to the N-terminus (residues 1–8), the central linker (between residues 75 and 111) and a basic loop in the FKBP domain (residues 156–162). By focusing on the conformationally rigid amides, we next determined the apparent size of the folded domains by measuring the ratio of ^{15}N T1 relaxation to ^{15}N T2 relaxation (Figure 7A). The results indicate different values for the BTHB (9±1) and the FKBP (15±3) domains. The relative magnitude of these values (1:1.7) are the same as their relative sizes (1:1.6; 70 residues versus 115 residues) which is consistent with motionally independent domains. If the two domains were structurally coupled they would instead share the same value. We also confirmed that the domains remain motionally independent upon association with the dsRNA-23 bp ligand (Supplementary Figure S9). To rule out more subtle and transient domain-domain contacts, we introduced cysteine mutants at various positions of full-length FKBP25 with the aim to attach a paramagnetic nitroxide spin-label to various locations guided by the previous model (Supplementary Figure S10A). In this technique, distances of up to 15–20 Å can be observed including those that are weak or transient in nature. Placement of the nitroxide to amino acid 14 and 69 resulted only in local effects within the BTHB domain (Figure 7B and Supplementary Figure S10B). In addition, placement of the nitroxide at amino acid 151 only affected spatially proximal residues within the PPIase domain. Taken together we find that the BTHB and FKBP domains are not fixed together, but are instead independent and connected only by the flexible linker (Figure 7C). This property will ensure that upon BTHB domain binding to dsRNA, the FKBP domain will retain motional freedom to interact with a range of nearby protein substrates.

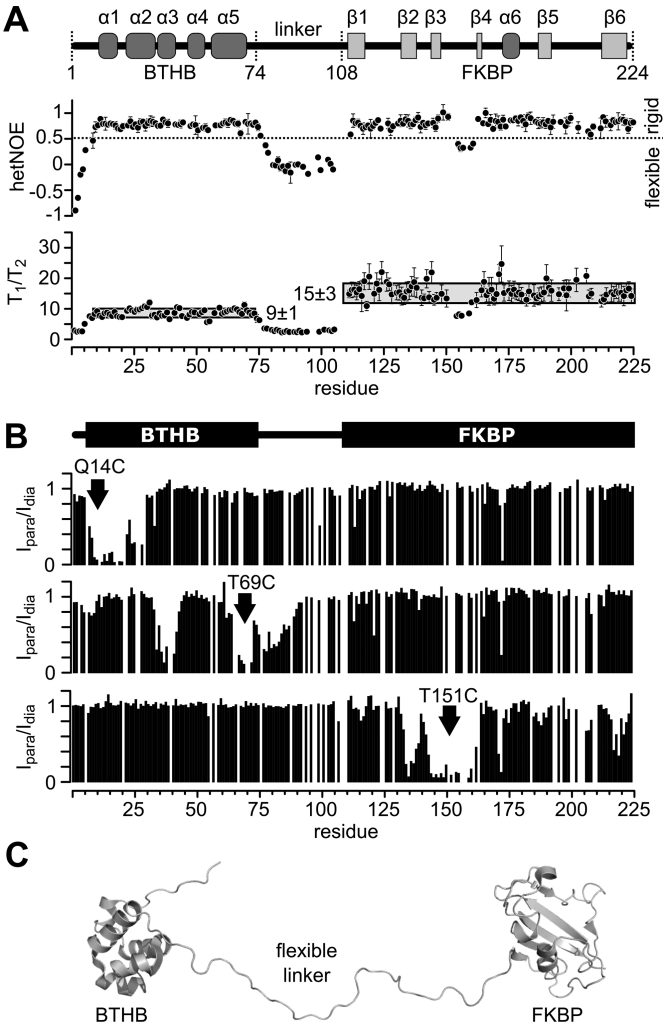

Figure 7. The BTHB and FKBP domains of FKBP25 are structurally independent. (**A**) ^{15}N relaxation measurements of ^{15}N-labelled FKBP25 at 298K using a 700 MHz NMR spectrometer. Heteronuclear $\{^1H\}^{15}N$ NOE measurements for backbone amide nitrogen identify residues that are conformationally rigid (values greater than 0.5) or flexible (less than 0.5) at the ps-ns timescale. The ratio of T1 over T2 values results with differing values of 9 ± 1 and 15 ± 3 for the BTHB and FKBP domains, respectively. The secondary structure of FKBP25 is illustrated at the top. (**B**) Incorporation of the nitroxide compound TEMPO to the FKBP25 mutant Q14C, T69C and T151C. Distance-dependent attenuation of crosspeak intensities caused by the paramagnetic nitroxide are shown, and are restricted to intra-domain effects. Full analysis in Supplementary Figure S6. (**C**) The two domains of FKBP25 do not form a single structural unit in solution, but are only connected by the flexible linker.

DISCUSSION

We have used a variety of techniques to demonstrate an RNA-dependent interaction of FKBP25 with several proteins involved in RNA metabolism; these include ribosome biogenesis and chromatin regulatory factors. We observe RNA-dependent nucleolar localization of FKBP25, which is consistent with a function of this protein in pre-ribosome assembly. Using a collection of NMR techniques, we show that this novel property of a prolyl isomerase is conferred by its N-terminal BTHB domain which is able to directly and selectively bind to dsRNA. These results thus identify FKBP25 as a peptidyl-prolyl isomerase recruited to ribonucleoprotein complexes.

Protein domains that specifically bind to dsRNA are not common. The most prominent example is the family of dsRNA-binding domain (dsRBD) proteins. The dsRBD is a small domain (usually 65–70 amino acids) containing both α-helices and β-strands in an α-β-β-β-α architecture (51). This domain is found in proteins that edit and process rRNA, tRNA, siRNA and miRNAs. In addition,

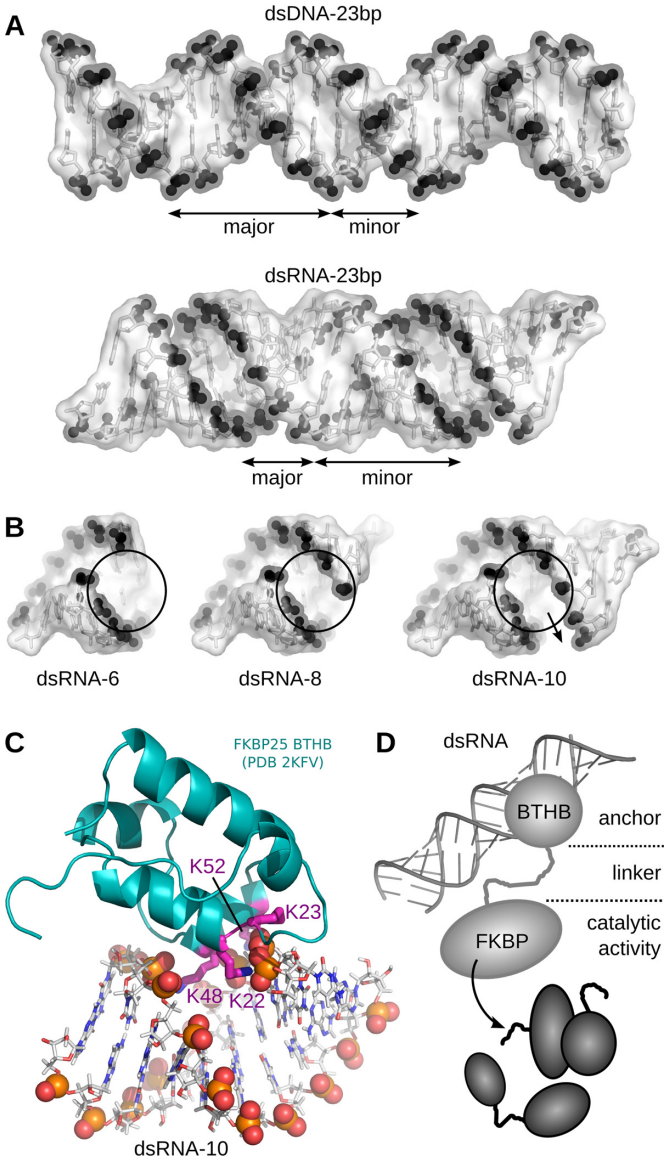

Figure 8. Model of FKBP25 interacting with dsRNA. (**A**) Surface representation of 23-bp dsDNA and dsRNA with main-chain phosphates coloured black and the major and minor grooves labeled. (**B**) Comparison of 6, 8 and 10 bp dsDNA ligands. Phosphates on opposing sides of the major groove require a minimum length of 8 bp. In longer ligands the BTHB domain is able to bind in multiple registers or slide along the major groove. (**C**) Docking model of BTHB bound to an A-form conformation of dsRNA-10. Further details in Supplementary Figure S7A. (**D**) Schematic model of FKBP25 bound to dsRNA.

dsRBD-containing proteins play a role in the protein kinase RNA-activated (PKR) response and mRNA localization, and dsRBDs are also found in bacterial endoribonucleases. In general, recognition of dsRNA by dsRBD is guided by the shape features unique to dsRNA. Compared to the canonical B-form dsDNA, dsRNA is typically found in the A-form with a narrower and deeper major groove and a wider and shallower minor groove (Figure 8A) (52). The dsRBD straddles contiguous minor-major-minor grooves, with shape recognition predominating the interaction but with some dsRBD members displaying sequence specificity with base pairs in the minor grooves. A central region of the dsRBD–dsRNA interface involves residues that contact phosphate groups on opposing sides of the major groove.

In our study of dsRNA binding by FKBP25, we show that a minimum length of 8 bp is required for association with the BTHB domain (Figure 5). A comparison of A-form dsRNA models explains this preference: it is evident that 8 and 10 bp ligands are sufficient in length to display phosphates on opposite sides of the major groove, whereas a dsRNA ligand of 6 bp is too short (Figure 8B). As a result, it is likely that the BTHB domain uses this feature of the major groove to specifically recognize dsRNA. Indeed, by using the dsRNA-10 ligand sequence and binding contribution by the key lysines K22, K23, K48 and K52, a docking-based (HADDOCK2.2) (53–55) model illustrates that the BTHB can efficiently interact with phosphates on both sides of the major groove (Figure 8C and Supplementary Figure S11A). This model of recognition is reminiscent of the central dsRBD interaction to the dsRNA major-groove (Supplementary Figure S11B).

The discovery of direct RNA-binding by FKBP25 provides an explanation for the dependence of RNA on protein–protein association and cellular localization. In addition, we show that the BTHB and FKBP are structurally independent. Together, these data support a model in which the BTHB domain recognizes dsRNA while retaining mobility of the FKBP domain to search out and interact with proximal proteins (Figure 8D).

A significant fraction of FKBP25 co-localizes with UBF and therefore with sites of active rRNA synthesis. This localization supports a role of FKBP25 in ribosome biogenesis in the nucleolus. As rRNA is processed, it is loaded with a variety of proteins in a highly-coordinated fashion (56). Because newly synthesized rRNA contains numerous stretches of accessible double-stranded RNA, including stemloop structures that interact with nucleolin (46,57,58), these nascent complexes are likely targets of this FKBP. Indeed, FKBP25 co-purifies with processed and semi-processed forms of 28S rRNA, but not mature ribosomes (21). The moderate affinity of FKBP25 for dsRNA would favour a high local concentration of FKBP25 to the regions of rRNA synthesis, but otherwise allow for movement within this compartment. In this scenario, a likely role for FKBP25 is to ensure proper folding or dynamics of ribosomal subunit proteins as they are assembling on the maturing 60S ribosome, by maintaining rapid isomerization of proline residues within their flexible loops and linkers. The ribosomal proteins identified in our BioID experiments are prime candidates for this regulation. In keeping with this function, FKBP25 is upregulated in regions of rapid cellular proliferation (59). This condition requires high levels of ribosome biogenesis and a mechanism by which to facilitate their assembly would be increasingly important. Conversely, growth arrest mediated by p53 activation is followed by downregulation of FKBP25 and decreased mRNA levels (60,61). Importantly, the high concentration of ribosomes may make FKBP25 interactions with the ribosomal (RPL) proteins the most detectable in the proximity labelling and co-immunoprecipitation methods that we have used. However, it is likely that other processes and protein complexes are also regulated by FKBP25. It will therefore be impor-

tant to determine if FKBP25 regulates other ribonucleoprotein complexes and cellular processes where dsRNA is involved. The GO enrichments categories of chromatin regulation, DNA repair and some cytoskeletal processes in our Bio-ID data provide some direction for these future investigations.

While there are several reports of cyclophilin and parvulin isomerases being linked to mRNA splicing (62), FKBP25 is so far the only FKBP family member that has demonstrated direct binding to RNA, and is the only prolyl isomerase shown to bind dsRNA. Interestingly, two cyclophilin prolyl isomerases are able to bind ssRNA due to an auxiliary RNA recognition motif (RRM) domain. The RRM domain of the nuclear human CYP33/PPIE directly binds to single-stranded AU-rich RNA sequences (63,64), such as mRNA, but does not bind to rRNA or tRNA (65). An overlapping interaction surface on the RRM domain also recognizes the third plant homeodomain (PHD3) of mixed lineage leukemia (MLL) protein, and the binding of MLL is thought to displace RNA (63). The second RNA-binding cyclophilin is CYP59/PPIL4 from *Arabidopsis thaliana,* which functions in pre-mRNA processing (66) and has both an RRM and zinc-knuckle domain. A binding preference for a G-U/C-N-G/A-C-C-A/G motif was determined, a sequence found in 70% of *Arabidopsis* protein-coding genes (67). There are no parvulin proteins that display RNA-binding behaviour. However, similar to FKBP25, human Par14/PIN4 has been implicated in ribosome biogenesis (68,69). Knockdown of cellular Par14 levels results in a decrease in the ribosome processing rate (68). In this case, the localization of Par14 appears to be due to association with nuclophosmin B23 or direct binding to DNA (68,70). Collectively, it appears that several prolyl isomerases are recruited to RNA-containing complexes, and this suggests that cis-trans prolyl isomerization of RNA proximal proteins is critical for their dynamic functions.

In terms of cellular localization, we note that most of the identified FKBP25 interactions (Figure 1) are in keeping with a predominantly nucleolar presence. However, it is also evident that FKBP25 is present within other regions of the cell. In the cytoplasm, FKBP25 may interact with a separate cohort of protein factors and perform different roles. Nevertheless, the ability to bind to regions of dsRNA could still represent a major factor in target recognition by FKBP25. For example, the identification of FKBP25 as a mRNA-binding protein (71) may represent interaction with regions of dsRNA such as stem–loop structures in cytosolic mRNA. Finally, it appears from the co-immunoprecipitation data that FKBP25 can also interact with a small number of proteins in an RNA-independent manner (Figure 1F). In this regard, other protein-protein interactions, or indeed the lower affinity of FKBP25 to DNA, may serve a more important role.

Although each FKBP family member likely has a restricted target repertoire, a clear preference for amino acids around the proline substrate has so far not been identified. This property is generally true for all three prolyl isomerase families (72,73), except for the protein Pin1 which recognizes a phosphorylated serine or threonine before the proline residue (74). Instead, cellular targets appear to be defined by domains such as the BTHB that limit the protein to a specific location or biomolecular complex. In this report, we reveal that FKBP25 is directed to ribonucleoprotein complexes via a novel dsRNA-binding domain. The continued characterization of these auxiliary domains will therefore help to identify the cellular targets of each proline isomerase, and enable a clearer understanding of their biological roles. This information will also provide a more detailed appreciation of the cellular processes and protein complexes that may be affected by immunosuppressive drugs of the cyclosporin and FK506/rapamycin families. A potential limitation of these drugs is that they target the catalytic domain, the part of the prolyl isomerase that displays reduced variation within each family. For example, given that FKBP12 and FKBP25 have a relatively similar affinity for rapamycin (75), our data suggest that ribosome biogenesis and other ribonucleoprotein complexes may be affected by the administration of rapamycin. Such additional, and possibly undesired, targets of these drugs could help explain unwanted side-effects. Instead of just targeting the shared isomerase domains, it is possible that auxiliary domains such as the BTHB may serve as effective and more precise targets of regulation.

DATA AVAILABILITY

Chemical shifts for the full-length and BTHB domains of FKBP25 have been deposited in the Biological Magnetic Resonance Data Bank under accession numbers 27070 and 27071.

SUPPLEMENTARY DATA

Supplementary Data are available at NAR Online.

ACKNOWLEDGEMENTS

We thank Brune Vialet for synthesis of the RNA oligonucleotides. Naoto Yamaguchi and Philippe Bouvet kindly provided plasmids. Access to NMR spectrometers, equipment and technical assistance were possible thanks to Axelle Grélard, Estelle Morvan and the structural biology platform at the Institut Européen de Chimie et Biologie (UMS 3033). NMR access was partially supported by the Centre Nationale de la Recherche Scientifique [IR-RMN-THC Fr3050]. European e-Infrastructure projects are acknowledged for the use of their web portals supported by FP7 WeNMR [project# 261572]; and H2020 West-Life [project# 675858].

FUNDING

French Canada Research Fund [C.J.N. and C.D.M.]; Fondation ARC for Cancer Research [PDF20111204271 to S.K.U.]; Canadian Breast Cancer Foundation BC/Yukon Branch [to C.J.N.]; Discovery Grant and Accelerator Supplement from the Natural Sciences and Engineering Research Council of Canada [to C.J.N.]. Funding for open access charge: Inserm.
Conflict of interest statement. None declared.

REFERENCES

1. Schmid,F.X. (1993) Prolyl isomerase: enzymatic catalysis of slow protein-folding reactions. *Annu. Rev. Biophys. Biomol. Struct.*, **22**, 123–142.
2. Schmid,F.X., Mayr,L.M., Mücke,M. and Schönbrunner,E.R. (1993) Prolyl isomerases: role in protein folding. *Adv. Protein Chem.*, **44**, 25–66.
3. Heitman,J., Movva,N.R. and Hall,M.N. (1992) Proline isomerases at the crossroads of protein folding, signal transduction, and immunosuppression. *New Biol.*, **4**, 448–460.
4. Sinkins,W.G., Goel,M., Estacion,M. and Schilling,W.P. (2004) Association of Immunophilins with Mammalian TRPC Channels. *J. Biol. Chem.*, **279**, 34521–34529.
5. Lummis,S.C.R., Beene,D.L., Lee,L.W., Lester,H.A., Broadhurst,R.W. and Dougherty,D.A. (2005) Cis–trans isomerization at a proline opens the pore of a neurotransmitter-gated ion channel. *Nature*, **438**, 248–252.
6. Lehnart,S.E., Huang,F., Marx,S.O. and Marks,A.R. (2003) Immunophilins and coupled gating of ryanodine receptors. *Curr. Top. Med. Chem.*, **3**, 1383–1391.
7. Colgan,J., Yuan,H.E., Franke,E.K. and Luban,J. (1996) Binding of the human immunodeficiency virus type 1 Gag polyprotein to cyclophilin A is mediated by the central region of capsid and requires Gag dimerization. *J. Virol.*, **70**, 4299–4310.
8. Gitti,R.K., Lee,B.M., Walker,J., Summers,M.F., Yoo,S. and Sundquist,W.I. (1996) Structure of the amino-terminal core domain of the HIV-1 capsid protein. *Science*, **273**, 231–235.
9. Minder,D., Böni,J., Schüpbach,J. and Gehring,H. (2002) Immunophilins and HIV-1 infection. *Arch. Virol.*, **147**, 1531–1542.
10. Brazin,K.N., Mallis,R.J., Fulton,D.B. and Andreotti,A.H. (2002) Regulation of the tyrosine kinase Itk by the peptidyl-prolyl isomerase cyclophilin A. *Proc. Natl. Acad. Sci. U.S.A.*, **99**, 1899–1904.
11. Wulf,G.M., Liou,Y.-C., Ryo,A., Lee,S.W. and Lu,K.P. (2002) Role of Pin1 in the regulation of p53 stability and p21 transactivation, and cell cycle checkpoints in response to DNA damage. *J. Biol. Chem.*, **277**, 47976–47979.
12. Rustighi,A., Tiberi,L., Soldano,A., Napoli,M., Nuciforo,P., Rosato,A., Kaplan,F., Capobianco,A., Pece,S., Di Fiore,P.P. *et al.* (2009) The prolyl-isomerase Pin1 is a Notch1 target that enhances Notch1 activation in cancer. *Nat. Cell Biol.*, **11**, 133–142.
13. Yang,W.M., Inouye,C.J. and Seto,E. (1995) Cyclophilin A and FKBP12 interact with YY1 and alter its transcriptional activity. *J. Biol. Chem.*, **270**, 15187–15193.
14. Yang,W.M., Yao,Y.L. and Seto,E. (2001) The FK506-binding protein 25 functionally associates with histone deacetylases and with transcription factor YY1. *EMBO J.*, **20**, 4814–4825.
15. Dilworth,D., Gudavicius,G., Leung,A. and Nelson,C.J. (2012) The roles of peptidyl-proline isomerases in gene regulation. *Biochem. Cell Biol.*, **90**, 55–69.
16. Nelson,C.J., Santos-Rosa,H. and Kouzarides,T. (2006) Proline isomerization of histone H3 regulates lysine methylation and gene expression. *Cell*, **126**, 905–916.
17. Park,S., Osmers,U., Raman,G., Schwantes,R.H., Diaz,M.O. and Bushweller,J.H. (2010) The PHD3 domain of MLL acts as a CYP33-regulated switch between MLL-mediated activation and repression, . *Biochemistry*, **49**, 6576–6586.
18. Li,H. and Luan,S. (2010) AtFKBP53 is a histone chaperone required for repression of ribosomal RNA gene expression in Arabidopsis. *Cell Res.*, **20**, 357–366.
19. Schiene-Fischer,C. (2015) Multidomain Peptidyl Prolyl cis/trans Isomerases. *Biochim. Biophys. Acta - Gen. Subj.*, **1850**, 2005–2016.
20. Jin,Y.J. and Burakoff,S.J. (1993) The 25-kDa FK506-binding protein is localized in the nucleus and associates with casein kinase II and nucleolin. *Proc. Natl. Acad. Sci. U.S.A.*, **90**, 7769–7773.
21. Gudavicius,G., Dilworth,D., Serpa,J.J., Sessler,N., Petrotchenko,E. V, Borchers,C.H. and Nelson,C.J. (2014) The prolyl isomerase, FKBP25, interacts with RNA-engaged nucleolin and the pre-60S ribosomal subunit. *RNA*, **20**, 1014–1022.
22. Ochocka,A.M., Kampanis,P., Nicol,S., Allende-Vega,N., Cox,M., Marcar,L., Milne,D., Fuller-Pace,F. and Meek,D. (2009) FKBP25, a novel regulator of the p53 pathway, induces the degradation of MDM2 and activation of p53. *FEBS Lett.*, **583**, 621–626.
23. Helander,S., Montecchio,M., Lemak,A., Farès,C., Almlöf,J., Li,Y., Yee,A., Arrowsmith,C.H., Dhe-Paganon,S. and Sunnerhagen,M. (2014) Basic tilted helix bundle—a new protein fold in human FKBP25/FKBP3 and HectD1. *Biochem. Biophys. Res. Commun.*, **447**, 26–31.
24. Prakash,A., Shin,J., Rajan,S. and Yoon,H.S. (2016) Structural basis of nucleic acid recognition by FK506-binding protein 25 (FKBP25), a nuclear immunophilin. *Nucleic Acids Res.*, **44**, 2909–2925.
25. Ishibashi,K., Fukumoto,Y., Hasegawa,H., Abe,K., Kubota,S., Aoyama,K., Kubota,S., Nakayama,Y. and Yamaguchi,N. (2013) Nuclear ErbB4 signaling through H3K9me3 is antagonized by EGFR-activated c-Src. *J. Cell Sci.*, **126**, 625–637.
26. Roux,K.J., Kim,D.I., Raida,M. and Burke,B. (2012) A promiscuous biotin ligase fusion protein identifies proximal and interacting proteins in mammalian cells. *J. Cell Biol.*, **196**. 801–810.
27. Mojica,S.A., Hovis,K.M., Frieman,M.B., Tran,B., Hsia,R., Ravel,J., Jenkins-Houk,C., Wilson,K.L. and Bavoil,P.M. (2015) SINC, a type III secreted protein of Chlamydia psittaci, targets the inner nuclear membrane of infected cells and uninfected neighbors. *Mol. Biol. Cell*, **26**, 1918–1934.
28. Mellacheruvu,D., Wright,Z., Couzens,A.L., Lambert,J.-P., St-Denis,N.A., Li,T., Miteva,Y. V, Hauri,S., Sardiu,M.E., Low,T.Y. *et al.* (2013) The CRAPome: a contaminant repository for affinity purification–mass spectrometry data. *Nat. Methods*, **10**, 730–736.
29. Huang,D.W., Sherman,B.T. and Lempicki,R.A. (2008) Systematic and integrative analysis of large gene lists using DAVID bioinformatics resources. *Nat. Protoc.*, **4**, 44–57.
30. Supek,F., Bošnjak,M., Škunca,N. and Šmuc,T. (2011) REVIGO summarizes and visualizes long lists of gene ontology terms. *PLoS One*, **6**, e21800.
31. Shannon,P., Markiel,A., Ozier,O., Baliga,N.S., Wang,J.T., Ramage,D., Amin,N., Schwikowski,B. and Ideker,T. (2003) Cytoscape: a software environment for integrated models of biomolecular interaction networks. *Genome Res.*, **13**, 2498–2504.
32. Alonso-López,D., Gutiérrez,M.A., Lopes,K.P., Prieto,C., Santamaría,R. and De Las Rivas,J. (2016) APID interactomes: providing proteome-based interactomes with controlled quality for multiple species and derived networks. *Nucleic Acids Res.*, **44**, W529–W535.
33. Britton,S., Coates,J. and Jackson,S.P. (2013) A new method for high-resolution imaging of Ku foci to decipher mechanisms of DNA double-strand break repair. *J. Cell Biol.*, **202**, 579–595.
34. Schindelin,J., Arganda-Carreras,I., Frise,E., Kaynig,V., Longair,M., Pietzsch,T., Preibisch,S., Rueden,C., Saalfeld,S., Schmid,B. *et al.* (2012) Fiji: an open-source platform for biological-image analysis. *Nat. Methods*, **9**, 676–682.
35. Delaglio,F., Grzesiek,S., Vuister,G.W., Zhu,G., Pfeifer,J. and Bax,A. (1995) NMRPipe: a multidimensional spectral processing system based on UNIX pipes. *J. Biomol. NMR*, **6**, 277–293.
36. Yakhnin,A. V., Yakhnin,H. and Babitzke,P. (2012) Gel mobility shift assays to detect protein–RNA interactions. *Methods Mol. Biol.*, **905**, 201–211.
37. Konig,J., Zarnack,K., Rot,G., Curk,T., Kayikci,M., Zupan,B., Turner,D.J., Luscombe,N.M. and Ule,J. (2011) iCLIP—transcriptome-wide mapping of protein-RNA interactions with individual nucleotide resolution. *J. Vis. Exp.*, **50**, e2638.
38. Farrow,N.A., Zhang,O., Forman-Kay,J.D. and Kay,L.E. (1994) A heteronuclear correlation experiment for simultaneous determination of 15N longitudinal decay and chemical exchange rates of systems in slow equilibrium. *J. Biomol. NMR*, **4**, 727–734.
39. Johnson,B.A. and Blevins,R.A. (1994) NMR View: a computer program for the visualization and analysis of NMR data. *J. Biomol. NMR*, **4**, 603–614.
40. Maison,C., Bailly,D., Peters,A.H.F.M., Quivy,J.-P., Roche,D., Taddei,A., Lachner,M., Jenuwein,T. and Almouzni,G. (2002) Higher-order structure in pericentric heterochromatin involves a distinct pattern of histone modification and an RNA component. *Nat. Genet.*, **30**, 329–334.
41. Javed,A., Zaidi,S.K., Gutierrez,S.E., Lengner,C.J., Harrington,K.S., Hovhannisyan,H., Cho,B.C., Pratap,J., Pockwinse,S.M., Montecino,M. *et al.* (2004) In situ immunofluorescence analysis: immunofluorescence microscopy. *Methods Mol. Biol.*, **285**, 23–28.
42. Boulon,S., Westman,B.J., Hutten,S., Boisvert,F.-M. and Lamond,A.I. (2010) The nucleolus under stress. *Mol. Cell*, **40**, 216–227.

43. McStay,B. and Grummt,I. (2008) The epigenetics of rRNA genes: from molecular to chromosome biology. *Annu. Rev. Cell Dev. Biol.*, **24**, 131–157.
44. Galat,A. and Thai,R. (2014) Rapamycin-binding FKBP25 associates with diverse proteins that form large intracellular entities. *Biochem. Biophys. Res. Commun.*, **450**, 1255–1260.
45. Rivière,S., Ménez,A. and Galat,A. (1993) On the localization of FKBP25 in T-lymphocytes. *FEBS Lett.*, **315**, 247–251.
46. Finger,L.D., Trantirek,L., Johansson,C. and Feigon,J. (2003) Solution structures of stem-loop RNAs that bind to the two N-terminal RNA-binding domains of nucleolin. *Nucleic Acids Res.*, **31**, 6461–6472.
47. Kelly,R.C., Jensen,D.E. and von Hippel,P.H. (1976) DNA "melting" proteins. IV. Fluorescence measurements of binding parameters for bacteriophage T4 gene 32-protein to mono-, oligo-, and polynucleotides. *J. Biol. Chem.*, **251**, 7240–7250.
48. Mackereth,C.D. and Sattler,M. (2012) Dynamics in multi-domain protein recognition of RNA. *Curr. Opin. Struct. Biol.*, **22**, 287–296.
49. König,J., Zarnack,K., Luscombe,N.M. and Ule,J. (2012) Protein-RNA interactions: new genomic technologies and perspectives. *Nat. Rev. Genet.*, **13**, 77–83.
50. Huppertz,I., Attig,J., D'Ambrogio,A., Easton,L.E., Sibley,C.R., Sugimoto,Y., Tajnik,M., König,J. and Ule,J. (2014) iCLIP: protein–RNA interactions at nucleotide resolution. *Methods*, **65**, 274–287.
51. Masliah,G., Barraud,P. and Allain,F.H.-T. (2012) RNA recognition by double-stranded RNA binding domains: a matter of shape and sequence. *Cell. Mol. Life Sci.*, **70**, 1875–1895.
52. Dickerson,R., Drew,H., Conner,B., Wing,R., Fratini,A. and Kopka,M. (1982) The anatomy of A-, B-, and Z-DNA. *Science*, **216**, 475–478.
53. van Zundert,G.C.P., Rodrigues,J.P.G.L.M., Trellet,M., Schmitz,C., Kastritis,P.L., Karaca,E., Melquiond,A.S.J., van Dijk,M., de Vries,S.J. and Bonvin,A.M.J.J. (2016) The HADDOCK2.2 web server: user-friendly integrative modeling of biomolecular complexes. *J. Mol. Biol.*, **428**, 720–725.
54. Wassenaar,T.A., van Dijk,M., Loureiro-Ferreira,N., van der Schot,G., de Vries,S.J., Schmitz,C., van der Zwan,J., Boelens,R., Giachetti,A., Ferella,L. *et al.* (2012) WeNMR: structural biology on the grid. *J. Grid Comput.*, **10**, 743–767.
55. Dominguez,C., Boelens,R. and Bonvin,A.M.J.J. (2003) HADDOCK: a protein−protein docking approach based on biochemical or biophysical information. *J. Am. Chem. Soc.*, **125**, 1731–1737.
56. Woolford,J.L. and Baserga,S.J. (2013) Ribosome Biogenesis in the Yeast Saccharomyces cerevisiae. *Genetics*, **195**, 643–681.
57. Allain,F.H.-T., Bouvet,P., Dieckmann,T. and Feigon,J. (2000) Molecular basis of sequence-specific recognition of pre-ribosomal RNA by nucleolin. *EMBO J.*, **19**, 6870–6881.
58. Ginisty,H., Sicard,H., Roger,B. and Bouvet,P. (1999) Structure and functions of nucleolin. *J. Cell Sci.*, **112**, 761–772.
59. Mas,C., Guimiot-Maloum,I., Guimiot,F., Khelfaoui,M., Nepote,V., Bourgeois,F., Boda,B., Levacher,B., Galat,A., Moalic,J.-M. *et al.* (2005) Molecular cloning and expression pattern of the Fkbp25 gene during cerebral cortical neurogenesis. *Gene Expr. Patterns*, **5**, 577–585.
60. Ahn,J., Murphy,M., Kratowicz,S., Wang,A., Levine,A.J. and George,D.L. (1999) Down-regulation of the stathmin/Op18 and FKBP25 genes following p53 induction. *Oncogene*, **18**, 5954–5958.
61. Murphy,M., Hinman,A. and Levine,A.J. (1996) Wild-type p53 negatively regulates the expression of a microtubule-associated protein. *Genes Dev.*, **10**, 2971–2980.
62. Mesa,A., Somarelli,J.A. and Herrera,R.J. (2008) Spliceosomal immunophilins. *FEBS Lett.*, **582**, 2345–2351.
63. Hom,R.A., Chang,P.-Y., Roy,S., Musselman,C.A., Glass,K.C., Selezneva,A.I., Gozani,O., Ismagilov,R.F., Cleary,M.L. and Kutateladze,T.G. (2010) Molecular mechanism of MLL PHD3 and RNA recognition by the Cyp33 RRM domain. *J. Mol. Biol.*, **400**, 145–154.
64. Mi,H., Kops,O., Zimmermann,E., Jäschke,A. and Tropschug,M. (1996) A nuclear RNA-binding cyclophilin in human T cells. *FEBS Lett.*, **398**, 201–205.
65. Wang,Y., Han,R., Zhang,W., Yuan,Y., Zhang,X., Long,Y. and Mi,H. (2008) Human CyP33 binds specifically to mRNA and binding stimulates PPIase activity of hCyP33. *FEBS Lett.*, **582**, 835–839.
66. Gullerova,M., Barta,A. and Lorkovic,Z.J. (2006) AtCyp59 is a multidomain cyclophilin from Arabidopsis thaliana that interacts with SR proteins and the C-terminal domain of the RNA polymerase II. *RNA*, **12**, 631–643.
67. Bannikova,O., Zywicki,M., Marquez,Y., Skrahina,T., Kalyna,M. and Barta,A. (2013) Identification of RNA targets for the nuclear multidomain cyclophilin atCyp59 and their effect on PPIase activity. *Nucleic Acids Res.*, **41**, 1783–1796.
68. Fujiyama-Nakamura,S., Yoshikawa,H., Homma,K., Hayano,T., Tsujimura-Takahashi,T., Izumikawa,K., Ishikawa,H., Miyazawa,N., Yanagida,M., Miura,Y. *et al.* (2009) Parvulin (Par14), a peptidyl-prolyl cis-trans isomerase, is a novel rRNA processing factor that evolved in the metazoan lineage. *Mol. Cell. Proteomics*, **8**, 1552–1565.
69. Fujiyama,S., Yanagida,M., Hayano,T., Miura,Y., Isobe,T., Takahashi,N., Uchida,T. and Takahashi,N. (2002) Isolation and proteomic characterization of human parvulin-associating preribosomal ribonucleoprotein complexes. *J. Biol. Chem.*, **277**, 23773–23780.
70. Saningong,A.D. and Bayer,P. (2015) Human DNA-binding peptidyl-prolyl cis/trans isomerase Par14 is cell cycle dependently expressed and associates with chromatin in vivo. *BMC Biochem.*, **16**, 4.
71. Castello,A., Fischer,B., Eichelbaum,K., Horos,R., Beckmann,B.M., Strein,C., Davey,N.E., Humphreys,D.T., Preiss,T., Steinmetz,L.M. *et al.* (2012) Insights into RNA biology from an atlas of mammalian mRNA-binding proteins. *Cell*, **149**, 1393–1406.
72. Schmidpeter,P.A.M., Unther Jahreis,G., Geitner,A.-J. and Schmid,F.X. (2011) Prolyl isomerases show low sequence specificity toward the residue following the proline. *Biochemistry*, **50**, 4796–4803.
73. Zoldaák,G., Aumuüller,T., Luücke,C., Hritz,J., Oostenbrink,C., Fischer,G. and Schmid,F.X. (2009) A library of fluorescent peptides for exploring the substrate specificities of prolylsomerases. *Biochemistry*, **48**, 10423–10436.
74. Yaffe,M.B., Schutkowski,M., Shen,M., Zhou,X.Z., Stukenberg,P.T., Rahfeld,J.-U., Xu,J., Kuang,J., Kirschner,M.W., Fischer,G. *et al.* (1997) Sequence-specific and phosphorylation-dependent proline isomerization: a potential mitotic regulatory mechanism. *Science*, **278**, 1957–1960.
75. Galat,A., Lane,W.S., Standaert,R.F. and Schreiber,S.L. (1992) A rapamycin-selective 25-kDa immunophilin. *Biochemistry*, **31**, 2427–2434.